PLANT SCIENCES

# Phase separation of HRLP regulates flowering time in *Arabidopsis*

**Yu Zhang[1,2], Sheng Fan[2], Changmei Hua[1], Zhi Wei Norman Teo[1,2], Jian Xuan Kiang[2], Lisha Shen[2]*, Hao Yu[1,2]***

Copyright © 2022 The Authors, some rights reserved; exclusive licensee American Association for the Advancement of Science. No claim to original U.S. Government Works. Distributed under a Creative Commons Attribution NonCommercial License 4.0 (CC BY-NC).

**RNA binding proteins mediate posttranscriptional RNA metabolism and play regulatory roles in many developmental processes in eukaryotes. Despite their known effects on the floral transition from vegetative to reproductive growth in plants, the underlying mechanisms remain largely obscure. Here, we show that a hitherto unknown RNA binding protein, hnRNP R-LIKE PROTEIN (HRLP), inhibits cotranscriptional splicing of a key floral repressor gene *FLOWERING LOCUS C* (*FLC*). This, in turn, facilitates R-loop formation near *FLC* intron I to repress its transcription, thereby promoting the floral transition in *Arabidopsis thaliana*. HRLP, together with the splicing factor ARGININE/SERINE-RICH 45, forms phase-separated nuclear condensates with liquid-like properties, which is essential for HRLP function in regulating *FLC* splicing, R-loop formation, and RNA Polymerase II recruitment. Our findings reveal that inhibition of cotranscriptional splicing of *FLC* by nuclear HRLP condensates constitutes the molecular basis for down-regulation of *FLC* transcript levels to ensure the reproductive success of *Arabidopsis*.**

## INTRODUCTION

Posttranscriptional regulation is an indispensable mechanism for controlling gene expression in eukaryotes. A nascent pre-mRNA transcript undergoes several tightly regulated RNA processing steps during or after transcription, including capping, splicing, modification, and polyadenylation, to form the mature mRNA before being exported to the cytoplasm for translation (*1*). All RNA processing events are mediated by the associated RNA binding proteins (RBPs), including the heterogeneous nuclear ribonucleoproteins (hnRNPs) representing a large family of RBPs that profoundly affect nearly every aspect of mRNA metabolism from transcription to RNA decay (*2*). The binding specificity and functional diversity of RBPs mostly rely on various combinations of RNA binding domains (RBDs) (*3*, *4*), such as the RNA recognition motif (RRM) (*5*), hnRNP K homology (KH) domain (*6*), and zinc finger domain (*7*), among which the RRM containing the two short conserved sequences, RNP1 and RNP2, is the most commonly found RBD (*4*, *8*). Although 196 RRM-containing RBPs have been annotated in the model plant *Arabidopsis thaliana* (*9*), most of them are yet to be functionally characterized.

RBPs play central regulatory roles in a multitude of diverse developmental and cellular processes in eukaryotes (*10*–*12*). In *Arabidopsis*, RBPs have been shown to affect the floral transition, a key developmental switch from vegetative to reproductive growth that determines the plant reproductive success (*10*, *13*, *14*). This transition is controlled by a complex network of genetic pathways in response to environmental and endogenous flowering signals (*13*). Several RBPs have been implicated to function in the autonomous pathway that monitors endogenous cues to affect the expression of *FLOWERING LOCUS C* (*FLC*), which encodes a potent floral repressor directly inhibiting the expression of two floral pathway integrators, *FLOWERING LOCUS T* (*FT*) and *SUPPRESSOR OF OVEREXPRESSION OF CONSTANS 1* (*SOC1*) (*15*–*17*). In particular, both the sense *FLC* transcript and alternative polyadenylation of the antisense *COOLAIR* transcripts from the *FLC* locus are modulated by two RBPs, FLOWERING CONTROL LOCUS A (FCA) and FPA, together with 3′ processing factors including FY, CLEAVAGE STIMULATING FACTOR 64 (CstF64), and CstF77 (*18*, *19*). Several other RBPs, such as RZ-1B, RZ-1C, SC35, and SC35-LIKE (SCL) proteins, have been shown to modulate splicing and expression of the sense *FLC* transcripts to regulate flowering (*20*, *21*). Single-molecule RNA fluorescence in situ hybridization (FISH) assay has revealed the colocalization of the nonspliced *FLC* RNA with *FLC* DNA FISH signals (*22*), implying that *FLC* pre-mRNA undergoes cotranscriptional splicing. Despite the above progress in understanding the effects of RBPs on *FLC* expression, the concrete mechanisms underlying cotranscriptional splicing at the *FLC* locus remain largely elusive.

Increasing evidence suggests that multiple RNA processing events occur within RBP-rich condensates, which are formed through phase separation driven by multivalent interactions between RNA and RBPs or intrinsically disordered regions (IDRs) of RBPs (*23*–*26*). Formation of protein condensates, including RBP-rich ones, have been shown to mediate multiple biological processes in plants, such as phytohormone signaling (*27*), flowering (*28*), intrachloroplast cargo sorting (*29*), thermosensory response (*30*), plant immune response (*31*), and microRNA processing (*32*). Notably, liquid-liquid phase separation (LLPS) of FCA promoted by FLX-LIKE 2 (FLL2) is crucial for FCA function in regulating the alternative polyadenylation of antisense *FLC* transcripts in flowering time control (*28*).

In this study, we reveal that a hitherto uncharacterized RBP, hnRNP R-LIKE PROTEIN (HRLP), plays a key role in suppressing cotranscriptional splicing of *FLC*, which enhances R-loop formation near *FLC* intron I, resulting in reduced recruitment of RNA Polymerase II (Pol II) and a consequential low *FLC* expression. HRLP, together with the splicing factor ARGININE/SERINE-RICH 45 (SR45), undergoes LLPS both in vitro and in vivo to form phase-separated nuclear condensates, which is required for inhibiting the cotranscriptional splicing process of *FLC*. In contrast, loss of HRLP or failure in forming HRLP nuclear bodies facilitates the cotranscriptional splicing and transcription of *FLC*, thus preventing the floral transition. Our study uncovers that inhibition of

[1]Department of Biological Sciences, Faculty of Science, National University of Singapore, Singapore 117543, Singapore. [2]Temasek Life Sciences Laboratory, National University of Singapore, Singapore 117604, Singapore.
*Corresponding author. Email: lisha@tll.org.sg (L.S.); dbsyuhao@nus.edu.sg (H.Y.)

cotranscriptional splicing of *FLC* by nuclear HRLP condensates is an integral mechanism underlying posttranscriptional regulation of *FLC* to determine the flowering time in *Arabidopsis*.

## RESULTS

### HRLP promotes flowering in *Arabidopsis*

HRLP (AT2G44710) is one of the *Arabidopsis* orthologs of the human hnRNP R (fig. S1) and shares high sequence similarity with its closest homologs in other plant species (fig. S2A). HRLP contains one coiled-coil domain, three RRMs, and multiple low-complexity regions (LCRs) as predicted by the Simple Modular Architecture Research Tool (SMART; fig. S2B). To study the biological function of HRLP, we obtained a mutant, *hrlp-1* (Salk_124411), harboring a T-DNA insertion in the fourth intron in the Columbia (Col-0) background from the *Arabidopsis* Biological Resource Center (Fig. 1A). This mutant, in which *HRLP* transcripts spanning the T-DNA insertion site were undetectable (fig. S3, A and B), displayed significantly late flowering compared with wild-type plants under both long days (LDs) and short days (SDs; Fig. 1, B to E). To confirm the role of *HRLP* in affecting flowering, we further generated another mutant by the CRISPR-Cas9–mediated gene editing using a single-guide RNA (sgRNA) that targeted a region within the first exon of *HRLP* (Fig. 1A). We subsequently identified one homozygous mutant without the CRISPR-Cas9 transgene, designated *hrlp-2*, that contained 1 base pair (bp) of guanine (G) deletion at 3 bp upstream of the protospacer adjacent motif (Fig. 1A). Similarly, *hrlp-2* showed a late-flowering phenotype comparable to *hrlp-1* under both LDs and SDs (Fig. 1, B to E). These results suggest that *HRLP* promotes flowering in *Arabidopsis*.

To verify that the flowering defect of *hrlp* mutants was caused by loss of *HRLP* function, we transformed *hrlp-2* mutants with a 5.0-kb *HRLP* genomic construct (*g4HA-HRLP*) including the 0.8-kb 5′ upstream region, the 3.7-kb coding sequence fused in frame with a *4HA* tag immediately after ATG plus introns, and the 0.5-kb 3′ untranslated region (fig. S3A). Most of the *hrlp-2 g4HA-HRLP* T1 transformants exhibited comparable flowering time to wild-type plants (Fig. 1F), demonstrating that loss of *HRLP* is responsible for the late-flowering phenotype of *hrlp-2*. We then selected one representative *hrlp-2 g4HA-HRLP* line that may contain the transgene at a single locus based on a 3:1 Mendelian segregation ratio for further investigation.

### HRLP is highly expressed in developing seedlings

Quantitative real-time polymerase chain reaction (qRT-PCR) revealed that *HRLP* mRNA was expressed in all tissues examined with the highest expression in rosette leaves (Fig. 2A). Its expression was gradually increased in developing seedlings during the floral transition occurring at 9 to 13 days after gemination under our growth conditions (Fig. 2B), which is consistent with *HRLP* function as a flowering promoter. To examine the expression pattern of HRLP protein, we generated the *gHRLP-GUS* reporter lines, in which the same genomic fragment used in *g4HA-HRLP* was translationally fused to the β-*glucuronidase* (*GUS*) reporter gene (fig. S3A). Most of the *gHRLP-GUS* transgenic lines exhibited similar staining patterns. HRLP-GUS signals were detectable intensively in shoot apices and young rosette leaves, but weakly in old rosette leaves in developing seedlings in the course of the floral transition (Fig. 2, C to F). GUS signals were also detected in cauline leaves, stamens of young floral buds, and siliques (Fig. 2, G to I). In general, the expression of *HRLP*

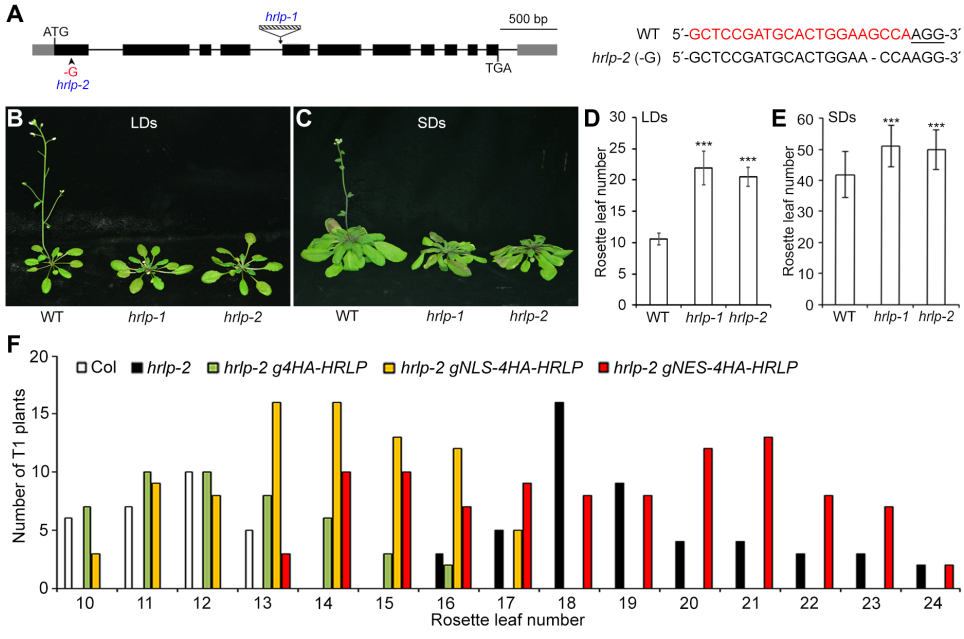


**Fig. 1. HRLP regulates flowering time in *Arabidopsis*.** (**A**) Schematic diagram shows the T-DNA insertion site in *hrlp-1* (Salk_124411) and the 1-bp G deletion site in *hrlp-2*. Exons in the coding region and untranslated regions (UTRs) are shown by black and gray boxes, respectively, and introns are indicated by black lines. The right panel shows the alignment of genomic DNA sequences of wild-type (WT) and *hrlp-2* containing the CRISPR-Cas9 target site. The 21-bp sgRNA sequence is shown in red color and the 3-bp protospacer adjacent motif is underlined. (**B** and **C**) *hrlp* mutants exhibit late flowering under LDs (B) and SDs (C). (**D** and **E**) Flowering time of *hrlp* mutants under LDs (D) and SDs (E). Error bars, means ± SD; $n = 20$. Asterisks indicate statistically significant differences between WT and *hrlp* plants (two-tailed paired Student's *t* test, ***$P < 0.001$). (**F**) Flowering time distribution of T1 transgenic plants of *hrlp-2 g4HA-HRLP*, *hrlp-2 gNLS-4HA-HRLP*, and *hrlp-2 gNES-4HA-HRLP*.

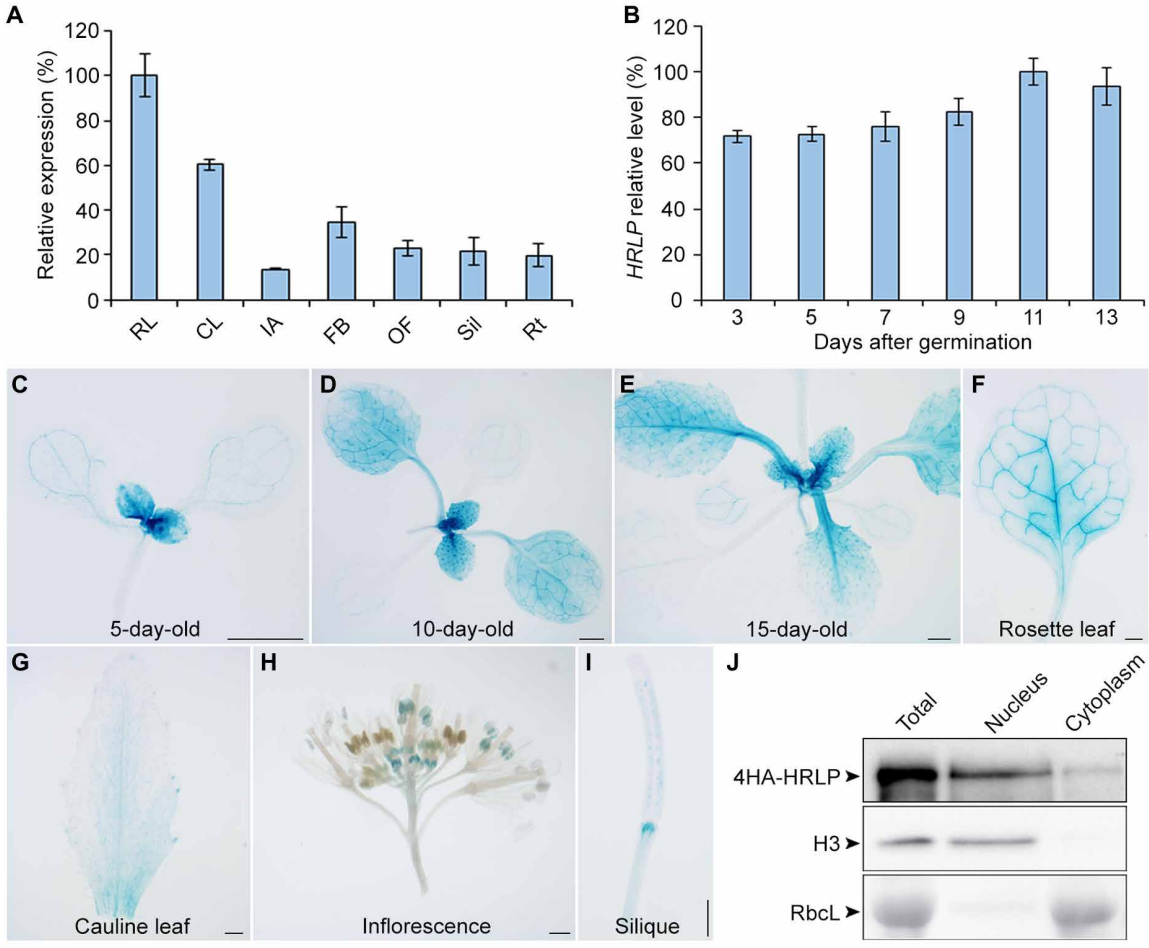


**Fig. 2. Expression pattern of *HRLP*.** (**A**) qRT-PCR analysis of *HRLP* expression in various tissues of WT Col plants. RL, rosette leaves; CL, cauline leaves; IA, inflorescence apices; FB, floral buds; OF, open flowers; Sil, siliques; Rt, roots. Levels of gene expression normalized to *TUB2* expression are shown relative to the maximal expression level set at 100%. Error bars, means ± SD; $n = 3$. (**B**) qRT-PCR analysis shows the temporal expression pattern of *HRLP* in WT seedlings from 3 to 13 days after germination under LDs. Levels of gene expression normalized to *TUB2* expression are shown relative to the maximal expression level set at 100%. Error bars, means ± SD; $n = 3$. (**C** to **I**) GUS staining of a representative *gHRLP-GUS* transgenic line reveals the *HRLP* expression pattern in a 5-day-old seedling (C), 10-day-old seedling (D), 15-day-old seedling (E), a rosette leaf (F), a cauline leaf (G), an inflorescence (H), and a silique (I). Scale bars, 1 mm. (**J**) HRLP is present in both nucleus and cytoplasm. Total, nuclear, and cytoplasmic proteins were extracted from 9-day-old *hrlp-2 g4HA-HRLP* seedlings and detected using anti-HA antibody. Histone 3 (H3) examined by anti-H3 antibody and the Rubisco large subunit (RbcL) stained with Ponceau S served as the internal controls for nuclear and cytosol fractions, respectively.

mRNA and HRLP-GUS protein was stronger in vegetative organs than reproductive organs.

To understand how *HRLP* affects flowering in response to various flowering signals, we analyzed *HRLP* expression in various flowering mutants and under different environmental conditions. *HRLP* expression levels were comparable in wild-type plants and mutants of the autonomous pathway, including *fca-2*, *fpa-7*, *flk-2*, *ld-1*, and *fld-3*, *fve-4* (fig. S3C), as well as the mutants of the photoperiod pathway, *gi-1*, *co-9*, and *ft-10* (fig. S3, D and E), indicating that *HRLP* expression is not regulated by the autonomous and photoperiod pathways. In addition, *hrlp-2* responded normally to the changes in ambient temperature (fig. S3F), implying that *HRLP* is not involved in the thermosensory pathway. *HRLP* expression was not obviously altered in the gibberellin (GA)–deficient mutant *ga1-3* compared with wild-type plants grown under SDs (fig. S3G). Moreover, GA treatment of *ga1-3* did not notably alter *HRLP* expression (fig. S3H), indicating that *HRLP* expression is not affected by the GA pathway. In contrast, although vernalization treatment of wild-type Col plants barely affected *HRLP* expression, vernalization treatment of *FRI FLC* significantly up-regulated *HRLP*, which was associated with the marked down-regulation of *FLC* (fig. S3, I and J). This observation implies that vernalization influences *HRLP* expression particularly when *FLC* expression levels are high.

To investigate the subcellular localization of HRLP, we examined HRLP protein levels in the nuclear and cytosolic fractions extracted from 9-day-old *hrlp-2 g4HA-HRLP* seedlings and found that 4HA-HRLP was present predominantly in the nucleus and weakly in the cytoplasm (Fig. 2J). To further explore which subcellular fraction of HRLP confers a promotive effect on flowering, we transformed *hrlp-2* with *gNLS-4HA-HRLP* and *gNES-4HA-HRLP* constructs, in which the nuclear localization signal (NLS) and the nuclear export signal (NES) were fused translationally with the start codon in the *g4HA-HRLP* construct, respectively (fig. S3A). Most of the *hrlp-2 gNLS-4HA-HRLP* lines showed earlier flowering than *hrlp-2*, whereas

most of the *hrlp-2 gNES-4HA-HRLP* lines exhibited late flowering like *hrlp-2* (Fig. 1F). Further immunoblot analysis revealed that NLS-4HA-HRLP and NES-4HA-HRLP proteins were exclusively localized in the nucleus and cytoplasm, respectively (fig. S3K). These results suggest that the nuclear HRLP plays a major role in promoting flowering.

### HRLP down-regulates *FLC* transcript levels

To explore the potential downstream targets of *HRLP* in regulating flowering time, we performed high-throughput sequencing of RNA extracted from 9-day-old wild-type and *hrlp-2* seedlings grown under LDs. Among these differentially expressed genes (fold change >2.0, $P < 0.05$) in *hrlp-2*, the expression levels of the key floral repressor *FLC* were evidently up-regulated (fig. S4A), which was in line with the late-flowering phenotype of *hrlp-2*. To verify the RNA sequencing (RNA-seq) result, we examined *FLC* expression in developing seedlings during the floral transition and again observed considerably up-regulated *FLC* transcript levels in *hrlp-2* versus wild-type plants (Fig. 3A). As *FLC* directly represses *FT* and *SOC1* expression (*33*), the expression of these two genes was consequently down-regulated in *hrlp-2* (Fig. 3, B and C). In contrast, the expression of the closest homologs of *FLC*, *MADS AFFECTING FLOWERING 1-5* (*MAF1-5*), and the FLC partner gene *SHORT VEGETATIVE PHASE* (*SVP*) was only slightly altered in *hrlp-2* during the floral transition (fig. S4, B to G). The above results were also corroborated by gene expression analyses in 9-day-old wild-type and *hrlp-1* seedlings (fig. S4H). Meanwhile, we also examined the expression of the *FLC* antisense transcript *COOLAIR* in *hrlp-2* mutants. Expression of the proximally polyadenylated class I *COOLAIR* remained unchanged, whereas expression of the distally polyadenylated class II *COOLAIR* was slightly increased in *hrlp-2* (fig. S4I). The latter could be associated with the increased *FLC* expression (*18*, *34*) rather than unaltered splicing of *COOLAIR* in *hrlp-2* (fig. S4J). In addition, the expression of several autonomous pathway genes acting upstream of *FLC*, including *FVE*, *FCA*, *FLD*, *FPA*, *LD*, *FLK*, and *FY*, were not affected by HRLP (fig. S4K). Together, these results imply that HRLP may directly modulate the *FLC* transcript levels to control flowering.

Furthermore, *flc-3* largely suppressed the late-flowering phenotype of *hrlp-1* and *hrlp-2* (Fig. 3, D and E, and fig. S4L), suggesting that the flowering defect of *hrlp* is mainly attributed to increased *FLC* levels. As expected, low expression levels of *SOC1* and *FT* in *hrlp-2* were restored in *flc-3 hrlp-2* to the extents similar to those in *flc-3* (Fig. 3F). These results suggest that HRLP promotes flowering mainly through modulating *FLC* transcript levels. The late-flowering phenotype of *hrlp-2* was still suppressed by vernalization treatment (fig. S4M), implying that the effect of vernalization on *FLC* expression is at least partially independent of HRLP.

### HRLP regulates splicing and transcription of *FLC*

Because RBPs affect almost all aspects of mRNA metabolism, including transcriptional and posttranscriptional processes (*1*, *2*), we proceeded to explore how HRLP affects *FLC* transcript levels during the floral transition. At the posttranscriptional level, we first examined the splicing efficiency of *FLC* by calculating the levels of each featured exons against those of their respective featured introns in *FLC* sense variants, *FLC.1-4* (Fig. 3G). The splicing efficiency of all featured introns of the four *FLC* isoforms except intron 6 of *FLC.3* was significantly increased in *hrlp-2*, especially for the major isoform *FLC.1* (Fig. 3G). Moreover, the splicing efficiency of *FLC* intron I was also significantly higher in *hrlp-2* than wild-type plants (Fig. 3G). These results indicate that HRLP negatively regulates the intron splicing of *FLC*. In contrast, HRLP did not affect the transcript stability or the nuclear-cytoplasmic transport of *FLC* mRNA (fig. S5, A and B). Next, we analyzed the abundance of nascent *FLC* transcripts to explore whether HRLP also regulates *FLC* at the transcriptional level. Nascent *FLC* RNA levels were significantly increased in *hrlp-2* compared with wild-type plants (Fig. 3H), indicating that HRLP also inhibits *FLC* transcription. Together, these results suggest that HRLP represses both splicing and transcription of *FLC*.

### HRLP is directly associated with *FLC* RNA

The nature of HRLP as an RBP with triple RRMs and its effects on suppressing splicing and transcription of *FLC* prompted us to examine whether HRLP is directly associated with *FLC* mRNA. In vitro RNA pull-down assay using the *FLC* mRNA probe showed that only glutathione *S*-transferase (GST)–HRLP(RRM) containing the triple RRMs of HRLP bound to the *FLC* probe, but not a *GFP* probe (fig. S5C), indicating that *FLC* mRNA bears the HRLP binding site(s). To determine the sequence preference for HRLP binding, we performed the systematic evolution of ligands by exponential enrichment (SELEX) experiment through screening sequences highly enriched with GST-HRLP versus GST (fig. S5, D and E) and identified the YUCCUY (Y=U/C) motif as a potential binding site for HRLP (Fig. 4A). We then carried out electrophoretic mobility shift assay (EMSA) using biotin-labeled RNA probes containing either four repeats of 5′-YUCCUY-3′ or four repeats of 5′-RAGGAR-3′ as a control. Only migration of the 5′-YUCCUY-3′ probe was retarded by GST-HRLP (Fig. 4B and fig. S5F), and this migration was weakened and even abolished by the addition of an increasing amount of the unlabeled probe (Fig. 4B). In addition, deletion of YUCCUY from *FLC* mRNA abolished its binding with GST-HRLP(RRM) (fig. S5, G and H). These observations strongly suggest that HRLP binds to the YUCCUY motif.

As there are nine YUCCUY motifs in the *FLC* pre-mRNA (Fig. 4C), we next investigated whether HRLP directly binds to *FLC* transcripts in vivo by RNA immunoprecipitation followed by qRT-PCR (RIP-qPCR) using the primers designed to cover the regions containing these YUCCUY motifs in the *FLC* pre-mRNA (Fig. 4C). RIP-qPCR performed on 9-day-old *hrlp-2 g4HA-HRLP* and *hrlp-2* seedlings revealed significant enrichment of HRLP on *FLC* pre-mRNA in *hrlp-2 g4HA-HRLP*, especially in the first exon and the first intron (Fig. 4C), suggesting a direct association of HRLP with *FLC* pre-mRNA in vivo.

### HRLP forms liquid-like nuclear condensate in vivo

To further elucidate the molecular mechanism by which HRLP modulates *FLC* splicing and transcription, we examined the distribution pattern of HRLP in the nucleus where HRLP functions in promoting flowering (Fig. 1F). HRLP–green fluorescent protein (GFP) was localized in multiple nuclear bodies in root tip cells of a functional *hrlp-2 gHRLP-GFP* line (Fig. 5A), in which the transgene bearing the *HRLP* genomic fragment translationally fused to the *GFP* reporter rescued the late-flowering phenotype of *hrlp-2* (fig. S6, A and B). Consistently, 4HA-HRLP was also localized in nuclear bodies in both leaf protoplasts (Fig. 5B) and root tip cells (fig. S6C) of *hrlp-2 g4HA-HRLP*. To test whether HRLP nuclear condensates display liquid-like characteristics, we performed the fluorescence

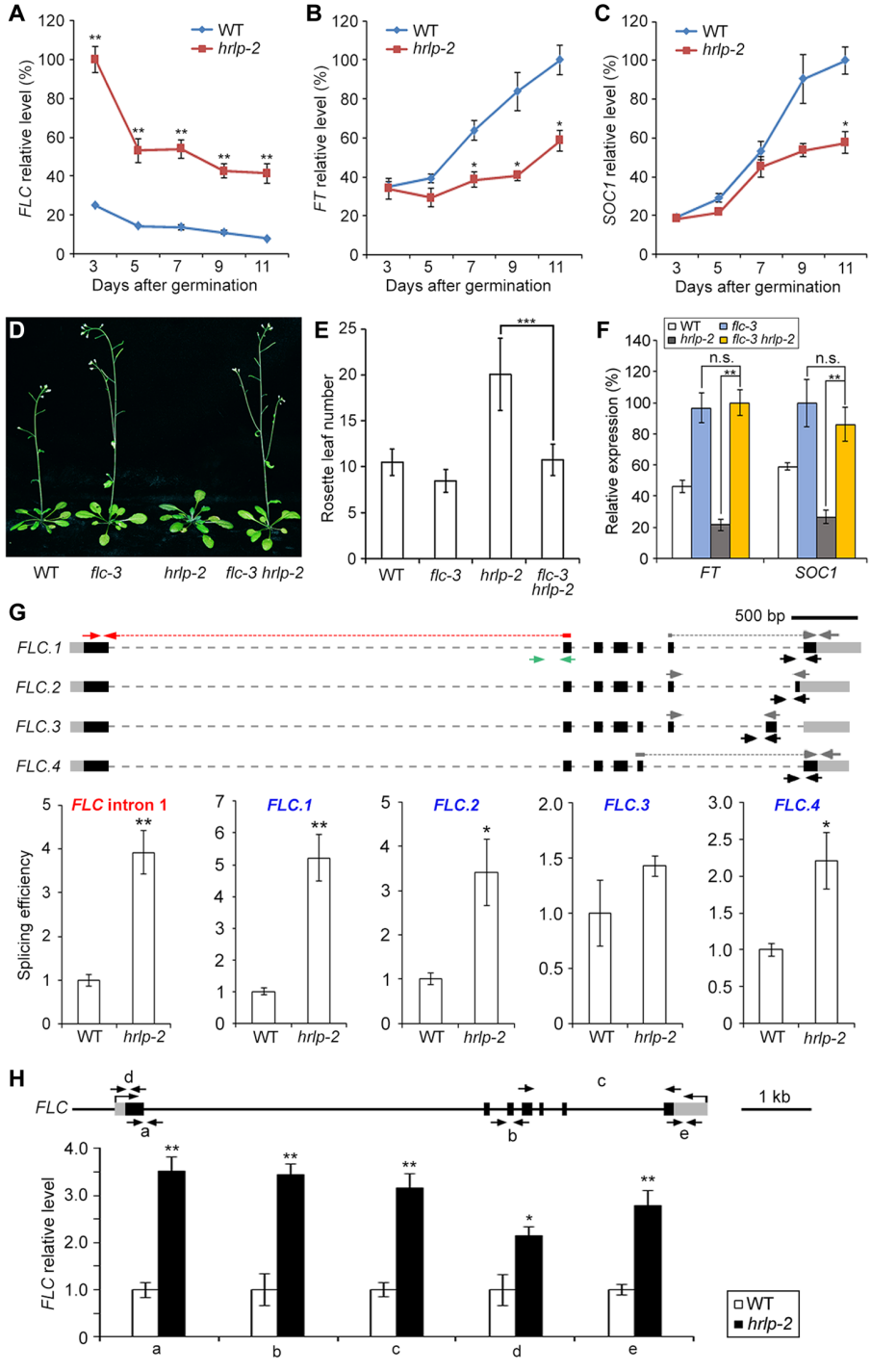


**Fig. 3. HRLP affects *FLC* transcripts levels.** (**A** to **C**) Expression of *FLC* (A), *FT* (B), and *SOC1* (C) in WT and *hrlp-2* seedlings under LDs. Gene expression levels in (A), (B), (C), and (F) normalized to *TUB2* expression are shown relative to the maximal level set at 100%. (**D**) Flowering phenotype of *flc-3*, *hrlp-2*, and *flc-3 hrlp-2*. (**E**) Flowering time of various plants under LDs. Error bars, means ± SD; $n = 20$. (**F**) Expression of *FT* and *SOC1* in various seedlings. (**G**) Splicing efficiency of *FLC* introns in 9-day-old WT and *hrlp-2* seedlings. The top panel shows schematic diagrams of *FLC* isoforms and primers for determining splicing efficiency. Black boxes, exons; gray boxes, UTRs; gray dashed lines, introns. Red arrows with dashed lines and green arrows indicate primers for exon I and intron I, respectively, while gray arrows with or without dashed lines and black arrows represent primers that determine other featured exons and the corresponding introns of each isoform, respectively. Splicing efficiency (bottom) was determined by normalizing expression levels of the featured exon against the corresponding unspliced alternative intron. The levels in WT plants are set as 1.0. (**H**) Nascent *FLC* levels in 9-day-old WT and *hrlp-2* seedlings. *FLC* genomic structure and primers for determining nascent *FLC* levels were shown above. Black lines, introns and upstream sequences; black boxes, exons; gray boxes, UTRs. Gene expression levels normalized to *EF1A* are shown relative to WT levels set as 1.0. Error bars (A, B, C, F, G, and H), means ± SD; $n = 3$. Asterisks indicate statistically significant differences between WT and *hrlp-2* plants (A, B, C, G, and H) or between indicated genotypes (E and F) (two-tailed paired Student's *t* test, $^*P < 0.05$, $^{**}P < 0.01$, and $^{***}P < 0.001$), whereas n.s. indicates no statistically significant differences ($P > 0.05$) (F).

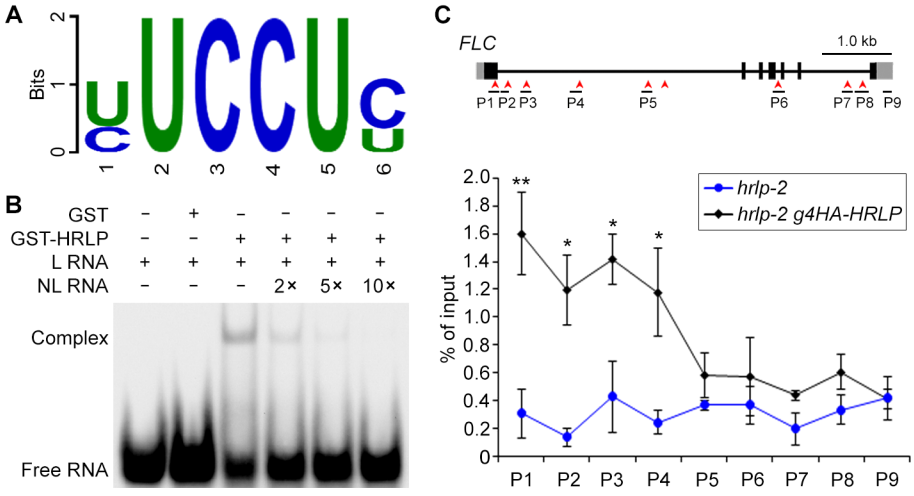


**Fig. 4. HRLP is directly associated with the *FLC* pre-mRNA.** (**A**) The sequence logo shows the mostly enriched motif associated with GST-HRLP in SELEX experiments. The size of the letter indicates the information content (measured in bits). (**B**) EMSA shows the in vitro binding of GST-HRLP to the YUCCUY motif. The RNA oligo containing four repeats of 5′-YUCCUY-3′ was used as the RNA probe. L RNA, labeled RNA probe; NL RNA, unlabeled RNA competitor. (**C**) RIP analysis using anti-HA antibody reveals the binding of HRLP to the *FLC* pre-mRNA in 9-day-old *hrlp-2 g4HA-HRLP* versus *hrlp-2* seedlings. The structure of *FLC* pre-mRNA and positions of 9 pairs of primers used in RIP assay are shown in the top panel. Red arrowheads indicate the positions of YUCCUY motifs. Exons, UTRs, and introns are indicated by black boxes, gray boxes, and black lines, respectively. Error bars, means ± SD; $n = 3$. Asterisks indicate statistically significant differences in HRLP association with *FLC* between *hrlp-2 g4HA-HRLP* and *hrlp-2* seedlings (two-tailed paired Student's *t* test, $^*P < 0.05$, $^{**}P < 0.01$).

recovery after photobleaching (FRAP) assay on HRLP-GFP nuclear bodies in *hrlp-2 gHRLP-GFP*. HRLP-GFP was rapidly redistributed from the unbleached area to the bleached area (Fig. 5, C and D), indicating a liquid-like state of HRLP condensates. Moreover, in *Nicotiana benthamiana* leaf epidermal cells transiently expressing *35S:GFP-HRLP*, GFP-HRLP was also localized in multiple nuclear bodies (Fig. 5E) and exhibited a similar liquid-like property under FRAP analysis (fig. S6, D and E). Together, these observations indicate that HRLP protein forms nuclear bodies with liquid-like properties via LLPS in vivo.

To investigate whether HRLP itself undergoes phase separation in vitro, we produced the recombinant GST-GFP-HRLP protein, from which the GST-tag was cleaved to generate GFP-HRLP. In the presence of PEG-8000 (polyethylene glycol, molecular weight 8000) as a crowding agent, GFP-HRLP, but not GFP, formed spherical droplets whose size gradually increased with increasing concentrations of GFP-HRLP proteins in a dosage-dependent manner (Fig. 5, F and G). FRAP assay further revealed that GFP-HRLP signals recovered shortly after photobleaching (Fig. 5, H and I), demonstrating that GFP-HRLP diffuses freely within the droplets. These results suggest that HRLP protein undergoes phase separation in vitro.

RBP condensate formation is often mediated by the IDRs containing high prevalence of glycine (G), arginine (R), lysine (K), or serine (S) residues (*23*, *25*, *35*–*37*). As predicted by SMART (fig. S6F), HRLP contains eight IDRs (IDR1 to IDR8), also called the LCRs, and the IDR(7&8) in the C-terminal region was recognized as a prion-like domain by PLACC (*38*). To identify the region(s) of HRLP conferring its phase separation feature, we first separated HRLP into two parts, the C-terminal part (HRLP-C) containing IDR(7&8) and the rest of the N-terminal part (HRLP-N; fig. S6G). Only GFP-HRLP-N formed nuclear bodies in *N. benthamiana* leaf epidermal cells (fig. S6H), indicating that the N-terminal part of HRLP is required for the phase separation of HRLP. We then divided HRLP-N into three regions, including HRLP(1-213) containing IDR (1-3), HRLP(214-473) containing the triple RRMs, and HRLP(474-727) containing IDR (4-6), among which only GFP-HRLP(474-727) was localized in nuclear bodies (fig. S6, G and H). Consistently, only GFP-HRLP(474-727) formed droplets in the presence of PEG-8000 in vitro (fig. S6I). We further dissected HRLP(474-727) and found that only GFP-HRLP(474-601) containing IDR(4&5) formed nuclear bodies, whereas neither IDR4 nor IDR5 itself was sufficient to drive nuclear body formation (fig. S6, G and H). These observations indicate that IDR(4&5) is required for phase separation of HRLP. As expected, the truncated HRLP without these two IDRs, GFP-HRLP(ΔIDR4&5), was expressed uniformly in the nucleus (Fig. 5J). Moreover, only the recombinant protein GFP-IDR(4&5), but not GFP-HRLP(ΔIDR4&5), formed droplets in vitro in the presence of PEG-8000 (Fig. 5K). FRAP assay subsequently detected a quick redistribution of GFP-IDR(4&5) from the unbleached area to the beached area after photobleaching (Fig. 5, L and M), suggesting that IDR(4&5) is sufficient for mediating phase separation. Together, these results demonstrate that IDR(4&5) is essential for the phase separation property of HRLP.

## Phase separation of HRLP promotes flowering

To assess the biological consequence of the phase separation of HRLP, we transformed *hrlp-2* with *GFP-HRLP* or *GFP-HRLP(ΔIDR4&5)* cDNA driven by the *HRLP* promoter. In the T1 generation, most of the *hrlp-2 pHRLP:GFP-HRLP* lines exhibited comparable flowering time to wild-type plants, whereas all *hrlp-2 pHRLP:GFP-HRLP(ΔIDR4&5)* lines exhibited late flowering like *hrlp-2* (Fig. 6A). This demonstrates that deletion of IDR(4&5) compromises HRLP's role in promoting flowering. We then selected representative *pHRLP:GFP-HRLP* and *pHRLP:GFP-HRLP(ΔIDR4&5)* lines that expressed GFP-HRLP and GFP-HRLP(ΔIDR4&5) mRNAs and proteins at similar levels (Fig. 6B and fig. S7, A and B) to observe their subcellular localization. In agreement with their localization in *N. benthamiana* leaf epidermal cells (Fig. 5, E and J), GFP-HRLP was localized in *pHRLP:GFP-HRLP*

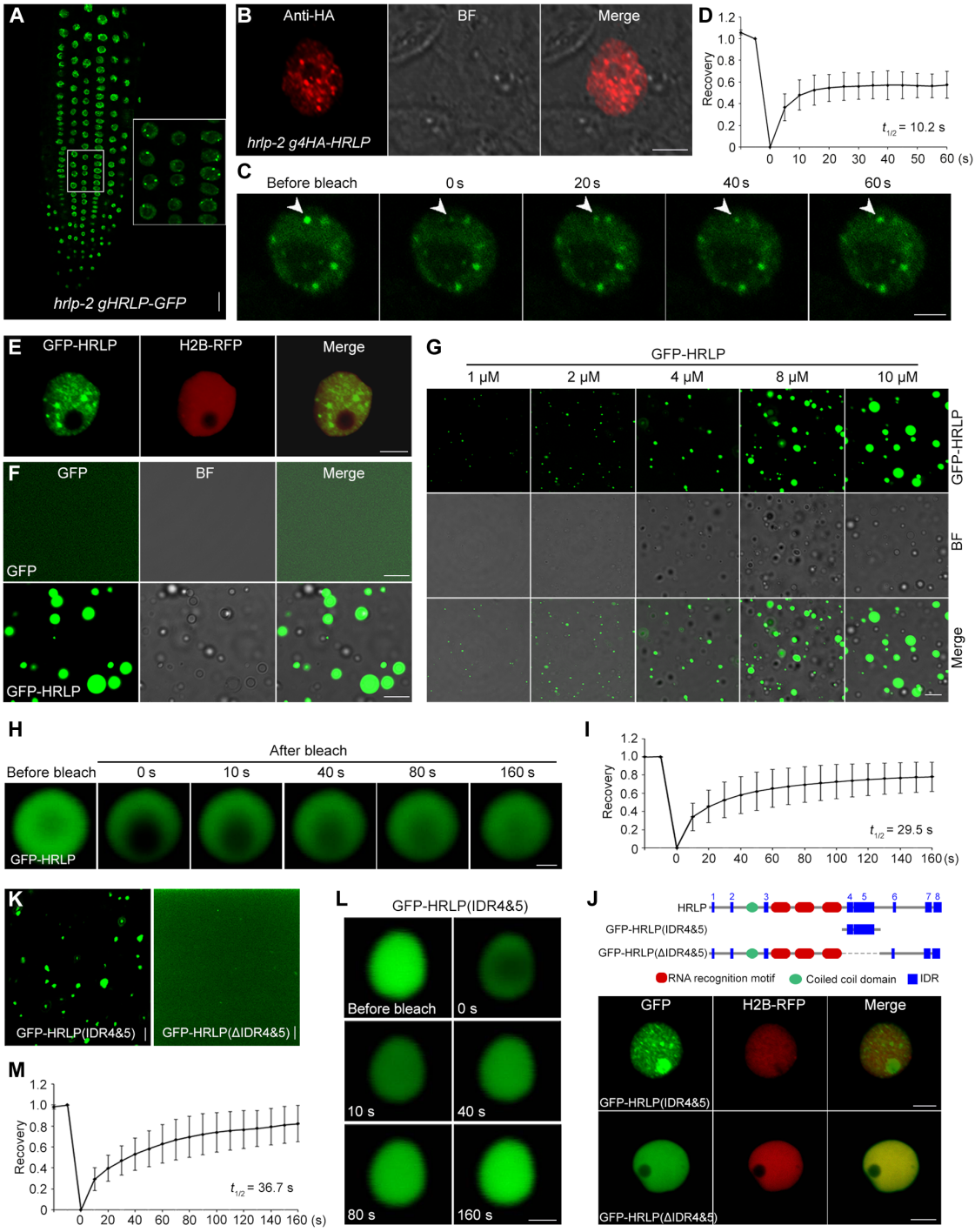


**Fig. 5. HRLP undergoes LLPS both in vitro and in vivo.** (**A**) HRLP-GFP localization in root tip cells of 5-day-old *hrlp-2 gHRLP-GFP* seedlings. Inset shows a magnified view. Scale bar, 20 μm. (**B**) Immunolocalization of 4HA-HRLP in an *hrlp-2 g4HA-HRLP* mesophyll protoplast. BF, bright field. Scale bar, 5 μm. (**C**) FRAP assay of an HRLP-GFP nuclear body (arrowheads) in *hrlp-2 gHRLP-GFP*. Time in (C), (H), and (L) indicates the duration after the photobleaching pulse. Scale bar, 5 μm. (**D**) FRAP recovery plot of HRLP-GFP nuclear bodies in *hrlp-2 gHRLP-GFP*. The value at the beginning of photobleaching in (D), (I), and (M) was set as 0. The half-time of recovery ($t_{1/2}$) in (D), (I), and (M) was calculated from the logarithmic curve and the best-fit values were generated by GraphPad. Error bars in (D), (I), and (M), means ± SD; $n = 15$. (**E**) Subcellular localization of GFP-HRLP in *N. benthamiana* leaf epidermal cells. H2B-RFP, RFP fluorescence of the nuclear reporter (core histone 2B fused to red fluorescent protein). Scale bar, 5 μm. (**F**) In vitro phase separation of GFP and GFP-HRLP proteins with the addition of PEG-8000. Scale bars, 10 μm. (**G**) Formation of droplets at the indicated concentrations of GFP-HRLP in the presence of PEG-8000 in vitro. Scale bar, 10 μm. (**H**) FRAP assay showing the recovery of GFP signals in a GFP-HRLP droplet. Scale bar, 1 μm. (**I**) FRAP recovery plot of GFP-HRLP droplets. (**J**) Subcellular localization of GFP-HRLP(IDR4&5) and GFP-HRLP(ΔIDR4&5) in *N. benthamiana* leaf epidermal cells. Scale bars, 5 μm. (**K**) In vitro phase separation of GFP-HRLP(IDR4&5) and GFP-HRLP(ΔIDR4&5) proteins with the addition of PEG-8000. Scale bars, 5 μm. (**L**) FRAP assay of a GFP-HRLP(IDR4&5) droplet. Scale bar, 1 μm. (**M**) FRAP recovery plot of GFP-HRLP(IDR4&5) droplets.

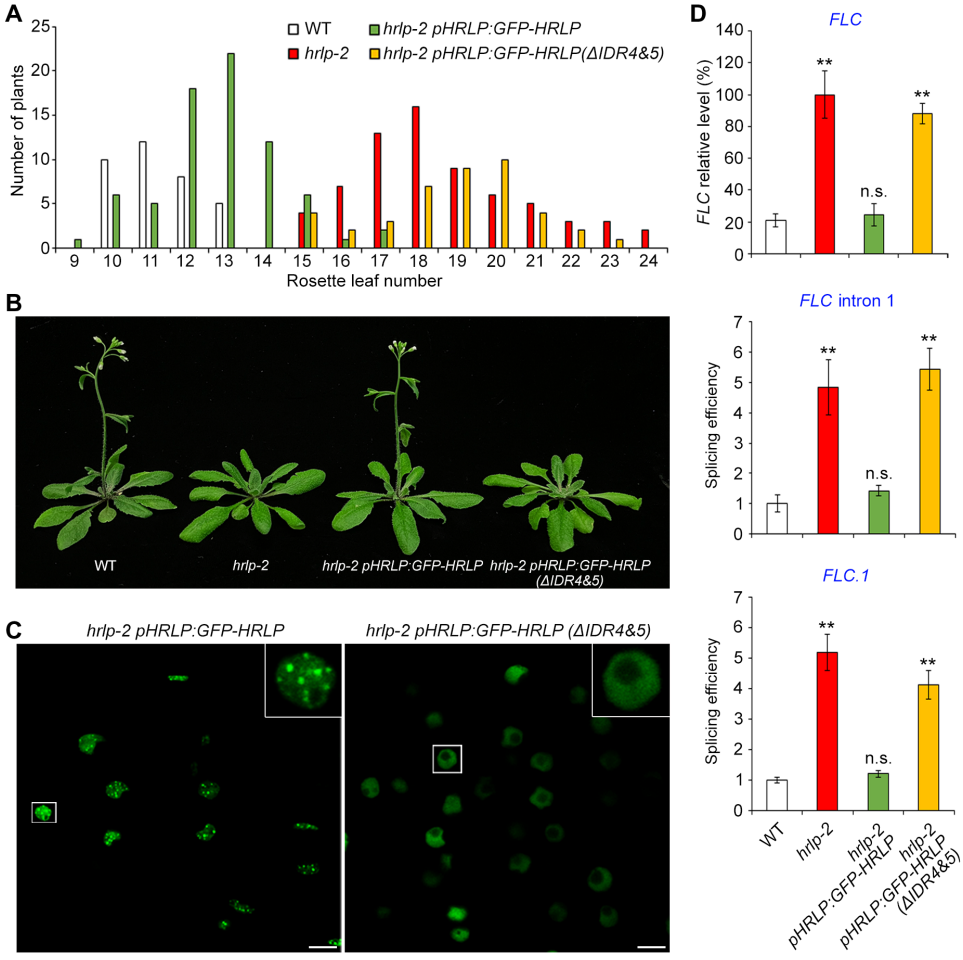


**Fig. 6. Phase separation of HRLP promotes flowering in *Arabidopsis*.** (**A**) Flowering time distribution of T1 transgenic plants of *hrlp-2 pHRLP:GFP-HRLP* and *hrlp-2 pHRLP:GFP-HRLP(ΔIDR4&5)*. (**B**) *pHRLP:GFP-HRLP(ΔIDR4&5)* is unable to rescue the late-flowering phenotype of *hrlp-2*. (**C**) Subcellular localization of GFP-HRLP and GFP-HRLP(ΔIDR4&5) in root tip cells of 5-day-old respective transgenic lines. The insets show enlarged images of the indicated nuclei in the white boxes. Scale bar, 10 μm. (**D**) *FLC* expression (top) and splicing efficiency of *FLC* intron I (middle) and intron 6 of *FLC.1* (bottom) in 9-day-old seedlings in different genetic backgrounds. *FLC* expression levels normalized to *TUB2* expression are shown relative to the maximal expression level set at 100%. The splicing efficiency was determined by normalizing the expression levels of the featured exon against the corresponding unspliced alternative intron of each isoform. The levels in WT plants are set as 1.0. Error bars, means ± SD; $n = 3$. Asterisks or n.s. indicate significant or no significant differences, respectively, between WT seedlings and the other genotypes (two-tailed paired Student's *t* test, $^{**}P < 0.01$; n.s., $P > 0.05$).

nuclear bodies, whereas GFP-HRLP(ΔIDR4&5) was distributed uniformly in *pHRLP:GFP-HRLP(ΔIDR4)&5)* nuclei (Fig. 6C). Moreover, overexpression of *GFP-HRLP* or *GFP-HRLP(ΔIDR4)&5)* cDNA in *hrlp-2* also revealed a similar link between phase separation of HRLP and its role in rescuing late flowering of *hrlp-2* (fig. S7, C and D). These observations suggest that phase separation of HRLP conferred by IDR(4&5) is critical for HRLP function in promoting flowering. Next, we examined whether phase separation of HRLP regulates *FLC* transcript levels and splicing efficiency of *FLC* introns. In line with the flowering behavior, both *FLC* expression and splicing were restored to the wild-type level in *hrlp-2 pHRLP:GFP-HRLP*, but not in *hrlp-2 pHRLP:GFP-HRLP(ΔIDR4&5)* (Fig. 6D). Single-molecule RNA FISH (smFISH) assay using smFISH probes against the *FLC* intron I sequence in *hrlp-2 gHRLP-GFP* also revealed that HRLP condensates were colocalized with *FLC* nascent transcripts (fig. S7E). These observations indicate that phase separation of HRLP is essential for its function in regulating *FLC* splicing and transcript levels. Overexpression of *GFP-HRLP(ΔIDR4&5)* in wild-type plants caused a late flowering phenotype (fig. S7F), indicating that overexpressed HRLP(ΔIDR4&5) could dominantly compete against wild-type HRLP for binding to *FLC*, thus possibly failing to suppress *FLC* expression.

## HRLP interacts with SR45 to modulate splicing and transcription of *FLC*

To uncover potential interacting partners in HRLP condensates, we performed coimmunoprecipitation (CoIP) assay followed by liquid chromatography–tandem mass spectrometry (LC-MS/MS) with *hrlp-2 g4HA-HRLP*. Notably, HRLP condensates were enriched with splicing factors, including SR45 (table S1), which is a plant-specific splicing factor involved in regulating *FLC* expression (*39*). We found that GFP-HRLP and SR45–red fluorescent protein (RFP) were colocalized in nuclear bodies in both *Arabidopsis* protoplasts and *N. benthamiana* leaf epidermal cells (fig. S8, A and B). CoIP assays in *N. benthamiana* confirmed the protein interaction between

HRLP1 and SR45 in vivo (fig. S8C). We generated *sr45-1 gSR45-3myc* transgenic plants, in which *gSR45-3myc* fully rescued the late-flowering phenotype of *sr45-1* (fig. S8D), and confirmed the interaction between HRLP and SR45 in *Arabidopsis* F1 seedlings from crosses between *sr45-1 gSR45-3myc* and *hrlp-2 g4HA-HRLP* (Fig. 7A). Bimolecular fluorescence complementation (BiFC) assays further revealed a direct interaction between HRLP and SR45 mainly in nuclear bodies (Fig. 7B). In addition, we found that SR45-RFP was incorporated into GFP-HRLP droplets (Fig. 7C and fig. S8, E and F), indicating that they may function together via phase separation. These results suggest that HRLP interacts with SR45 in nuclear bodies.

Similar to *hrlp* mutants, *sr45-1* exhibited a late-flowering phenotype (fig. S8, D and G) as previously reported (*39*). In *sr45-1* mutants, *FLC* transcript levels were up-regulated during the floral transition, whereas the expression of *FT* and *SOC1* was down-regulated (Fig. 7D and fig. S8H). We also found that the splicing efficiency of *FLC* intron I and the featured introns of the three *FLC* isoforms (*FLC.1,2,4*) was significantly higher in *sr45-1* than wild-type plants (Fig. 7, E and F). Moreover, nascent *FLC* levels were also considerably increased in *sr45-1* compared with wild-type plants (Fig. 7G). These effects of SR45 on *FLC* are mostly similar to those displayed by HRLP (Fig. 3), supporting the idea that HRLP interacts with SR45 to regulate *FLC* splicing and transcription. We further generated *sr45-1 hrlp-2* double mutants and found that *sr45-1 hrlp-2* double mutants flowered only slightly later than their single mutants (fig. S8I), supporting the notion that HRLP and SR45 function in a protein complex in regulating flowering.

### Phase separation of HRLP affects R-loop formation and RNA Pol II recruitment at *FLC*

Because the formation of DNA:RNA hybrids (R-loops) has been reported to affect gene expression, including the transcription at the *FLC* locus (*40*–*43*), we further tested whether the effects of HRLP and SR45 on *FLC* are relevant to cotranscriptional R-loop formation. DNA-RNA hybrid immunoprecipitation (DRIP) assay on 9-day-old seedlings revealed potential R-loop formation in the region spanning the first exon and the first intron (P1 to P3) as well as the region near the transcription termination site (P9 and P10) (Fig. 7H), which largely overlap with the regions reported in previous studies (*42*–*44*). Further R-loop foot-printing assay confirmed the R-loop formation in the first exon and intron of *FLC* (fig. S8J). Notably, high levels of R-loops in the region near intron I (P1 and P2) were significantly reduced in both *hrlp-2* and *sr45-1* mutants (Fig. 7I), but not in *FRI FLC* (fig. S8K) where *FLC* is highly expressed, but its splicing efficiency is not altered (*45*). To test whether this reduction of R-loops is correlated to RNA Pol II function as implicated in a previous study (*41*), we compared Pol II occupation at the *FLC* locus in *hrlp-2* and *sr45-1* mutants versus wild-type plants through chromatin immunoprecipitation (ChIP) assay using an antibody recognizing the C-terminal domain (CTD) of Pol II (anti-Pol II CTD). RNA Pol II enrichment at the region near intron I (P1 to P3) was increased in both *hrlp-2* and *sr45-1* versus wild-type plants, indicating that recruitment of RNA Pol II at the *FLC* locus is enhanced in *hrlp-2* and *sr45-1*. Together, these results suggest that HRLP and SR45 inhibit splicing and transcription of *FLC*, which is associated with R-loop formation and impediment of RNA Pol II recruitment in the region near intron I.

To assess whether phase separation of HRLP affects R-loop formation and RNA Pol II recruitment at the *FLC* locus, we examined R-loop formation at *FLC* in 9-day-old *hrlp-2 pHRLP:GFP-HRLP* and *hrlp-2 pHRLP:GFP-HRLP(ΔIDR4&5)* seedlings. DRIP assay showed high levels of R-loops in the region near intron I (P1 and P2) in both wild-type and *hrlp-2 pHRLP:GFP-HRLP* seedlings, whereas R-loop formation in the same region was significantly reduced in *hrlp-2* and *hrlp-2 pHRLP:GFP-HRLP(ΔIDR4&5)* (Fig. 8A). ChIP assay further revealed that RNA Pol II enrichment in the region near intron I (P1 to P3) was increased in *hrlp-2* and *hrlp-2 pHRLP:GFP-HRLP(ΔIDR4&5)* compared with wild-type and *hrlp-2 pHRLP:GFP-HRLP* seedlings (Fig. 8B). These findings, together with the observations on the effect of phase separation of HRLP on *FLC* splicing and transcript levels (Fig. 6D), suggest that phase separation of HRLP mediated by IDR(4&5) is crucial for its regulation of *FLC* mRNA levels.

## DISCUSSION

Throughout the life cycle of mRNA molecules, they are associated and modulated by diverse RBPs that influence all aspects of RNA metabolism, including RNA synthesis, splicing, modification, transport, translation, and degradation (*1*, *46*). Recent studies have suggested that a complex and complicated transcriptome control involving a large number of RBPs and their associated proteins possibly facilitates plants to evolve with more flexible and resilient strategies to cope with an ever-changing environment (*10*, *14*, *47*). Although, by now, more than 800 RBPs have been identified in *Arabidopsis* (*14*), their biological functions are largely unknown. In this study, we have shown that the plant hnRNP R-like RBP, HRLP, acts with the splicing factor SR45 to promote flowering through inhibiting the cotranscriptional splicing of the key flowering repressor *FLC*, which is associated with increased R-loop formation near its intron I to repress its transcription (Fig. 8C). This promotive effect of HRLP on flowering requires a liquid-like property conferred by its IDRs. Thus, HRLP condensate–mediated regulation of *FLC* splicing and transcription constitutes a hitherto unknown regulatory module that down-regulates *FLC* transcript levels to facilitate flowering under favorable conditions.

Our findings establish HRLP as a previously uncharacterized flowering promoter in modulating *FLC* mRNA levels. First, *hrlp* mutants exhibit a daylength-insensitive late-flowering phenotype under both LDs and SDs. *HRLP* expression is not obviously affected by most flowering genetic pathways tested, but positively regulated by vernalization in the presence of high *FLC* levels. Second, *FLC* transcripts are greatly increased in *hrlp* mutants, while *flc-3* almost completely suppresses the late-flowering phenotype of *hrlp*, suggesting that *FLC* is the major target of HRLP during the floral transition. Third, HRLP significantly reduces the splicing efficiency and transcription of *FLC* pre-mRNA via direct binding to its exon I and intron I. Moreover, HRLP interacts with the splicing factor SR45, which also down-regulates the splicing efficiency and transcription of *FLC* to promote flowering. In addition, because there are two other HRLP homolog proteins in the *Arabidopsis* genome, it would be interesting to investigate whether HRLP homologs also function in modulating *FLC* transcript levels in flowering time control.

Mounting evidence suggests that the processes of transcription and splicing are tightly coupled and mutually influence each other (*48*, *49*). For example, transcription elongation rate regulates alternative splicing, which, in turn, can also affect transcription (*50*–*54*). *FLC* pre-mRNA undergoes cotranscriptional splicing, as evident by

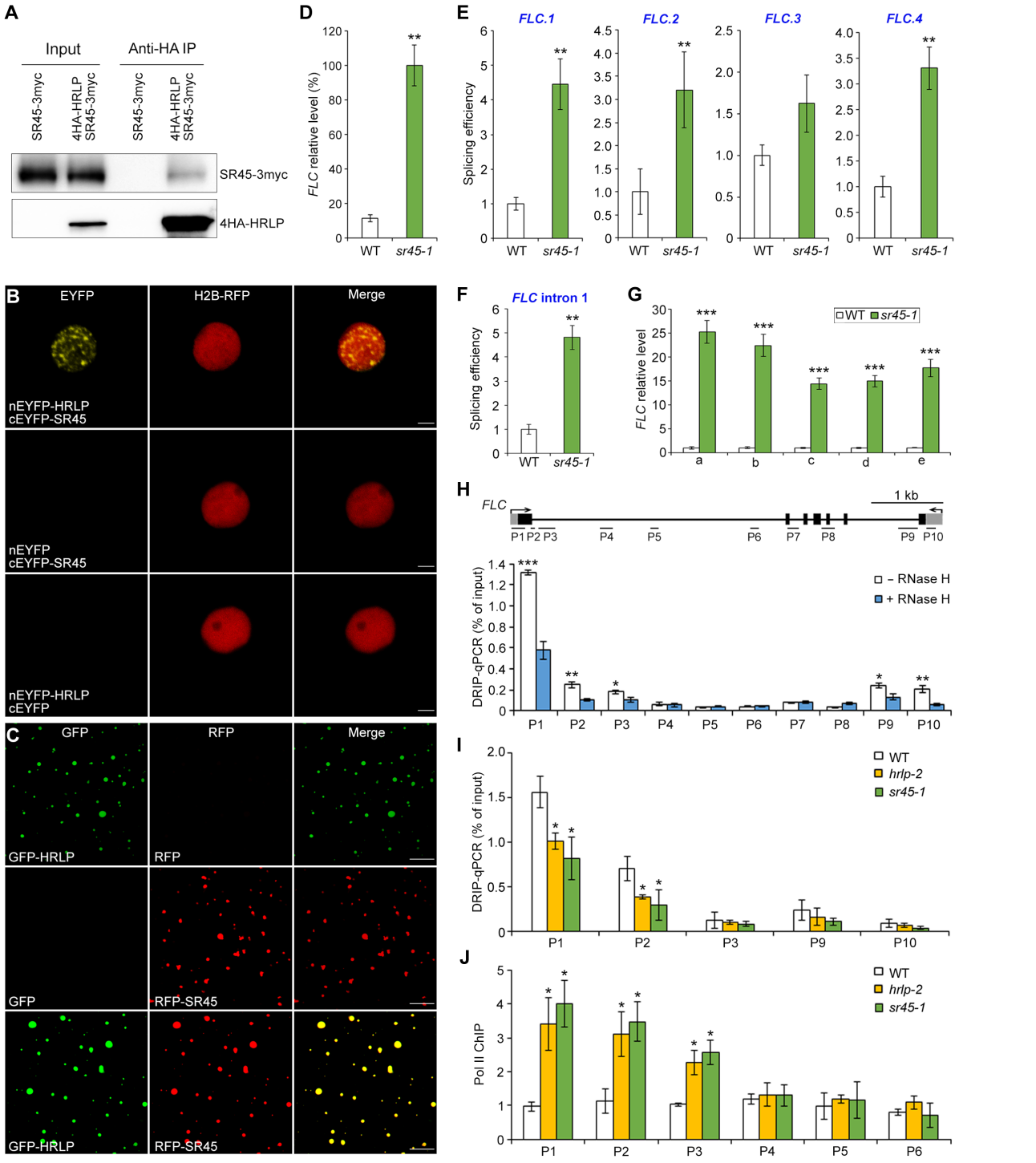


**Fig. 7. HRLP, together with SR45, regulates R-loop levels of *FLC*.** (**A**) CoIP shows the interaction between HRLP and SR45 in F1 seedlings from crosses between *sr45-1 gSR45-3myc* and *hrlp-2 g4HA-HRLP*. Proteins were detected by anti-myc (top) or anti-HA (bottom) antibodies. (**B**) BiFC analysis of the interaction between HRLP and SR45. Scale bars, 10 μm. (**C**) In vitro phase separation of 10 μM GFP-HRLP and RFP-SR45 proteins with the addition of PEG-8000. Scale bars, 10 μm. (**D**) Expression of *FLC* normalized to *TUB2* in 9-day-old WT and *sr45-1* seedlings. (**E** and **F**) Splicing efficiency of intron 6 of *FLC.1*, *FLC.2* and *FLC.3*, and intron 5 of *FLC.4* (E) and *FLC* intron I (F) in 9-day-old WT and *sr45-1* seedlings. Primer positions are indicated in Fig. 3G. (**G**) Measurement of nascent *FLC* levels in 9-day-old WT and *sr45-1* seedlings. Levels of gene expression normalized to *EF1A* expression are shown relative to WT expression levels set as 1.0. The positions of primers are shown in Fig. 3H. (**H**) DRIP analysis of R-loop formation at the *FLC* locus in 9-day-old WT seedlings with (+) and without (–) RNase H treatment. The gene structure of *FLC* and positions of primers used are shown in the top panel. (**I**) DRIP analysis of R-loop at the *FLC* locus in 9-day-old WT, *hrlp-2* and *sr45-1* seedlings. (**J**) Chromatin immunoprecipitation (ChIP) analysis of RNA Pol II enrichment at the *FLC* locus in 9-day-old WT, *hrlp-2*, and *sr45-1* seedlings. Error bars (D to J), means ± SD; $n = 3$. Asterisks (D to J) indicate significant differences between WT and mutants or between untreated and treated seedlings (two-tailed paired Student's *t* test, $^{*}P < 0.05$, $^{**}P < 0.01$, and $^{***}P < 0.001$).

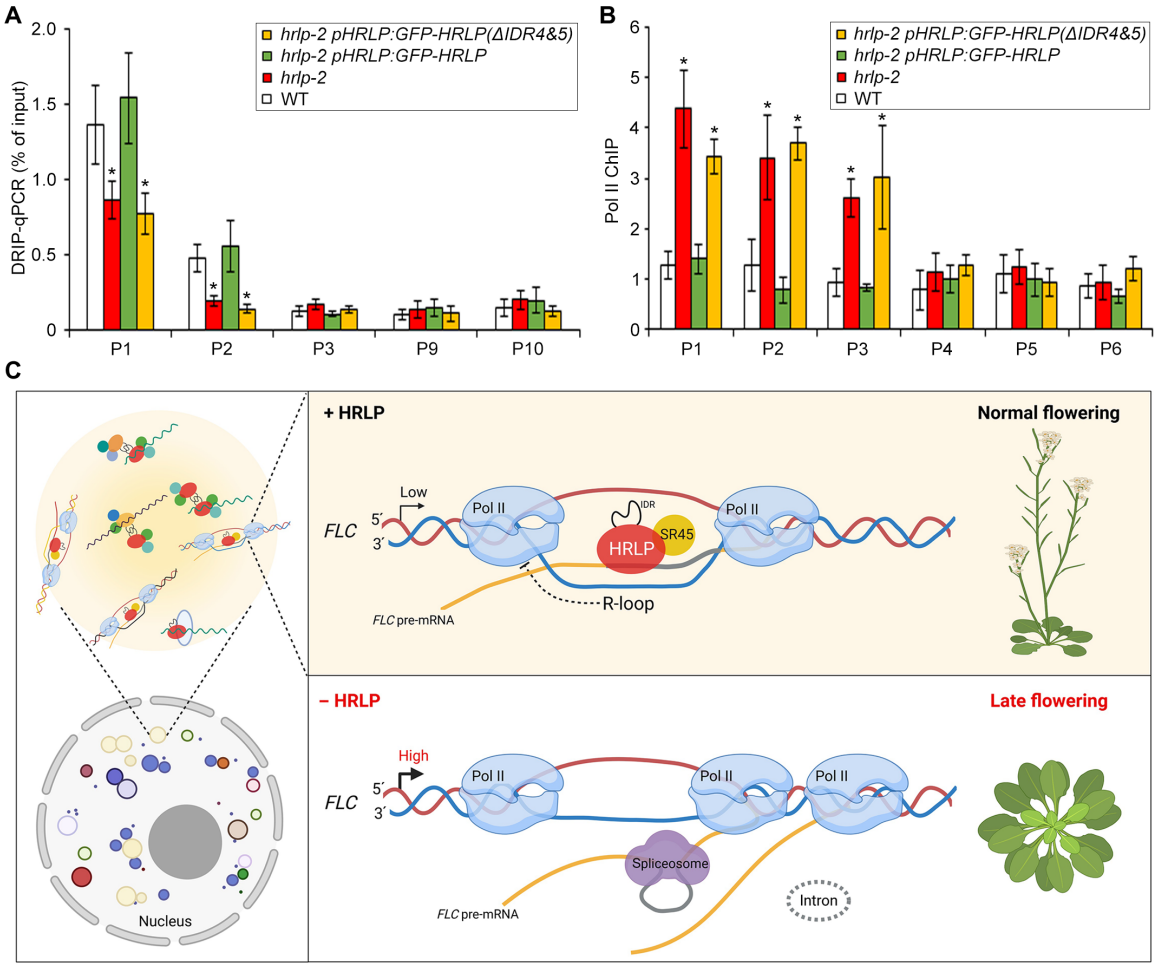


**Fig. 8. Phase separation of HRLP affects R-loop formation and RNA Pol II recruitment at the *FLC* locus.** (**A**) DRIP analysis of R-loop at the *FLC* locus in 9-day-old seedlings in various genetic backgrounds. (**B**) ChIP analysis of the enrichment of RNA Pol II over the genomic region of *FLC* in 9-day-old seedlings in various genetic backgrounds. In (A) and (B), error bars, means ± SD; $n = 3$. Asterisks indicate significant differences between WT plants and other specified genotypes (two-tailed paired Student's *t* test, $^*P < 0.05$). (**C**) A model depicting regulation of the cotranscriptional splicing of *FLC* by HRLP via phase separation. HRLP, together with SR45, is recruited to the region near intron I of the nascent *FLC* RNA by forming nuclear bodies to inhibit the splicing process, which enhances R-loop formation and compromises Pol II recruitment near intron I, thus suppressing *FLC* transcription. Loss of HRLP or failure in forming HRLP nuclear bodies enables cotranscriptional splicing of *FLC* introns. This compromises R-loop formation and facilitates recruitment of Pol II near intron I of *FLC*, resulting in higher *FLC* mRNA levels and the late-flowering phenotype. Created with BioRender.com.

the single molecular FISH analysis showing the colocalization of nonspliced *FLC* pre-mRNA with *FLC* DNA (*22*). Loss of *HRLP* or *SR45* leads to enhanced splicing efficiency and transcription of *FLC* pre-mRNA, which is coupled with reduced R-loop formation near *FLC* intron I, suggesting that HRLP-mediated inhibition of cotranscriptional splicing of *FLC* may alter the local chromatin context, thereby regulating *FLC* transcription. We have observed increased Pol II occupancy in *hrlp* or *sr45* mutants, particularly in the region near intron I where R-loop formation is reduced. Two ALBA family members, ALBA4 and ALBA5, whose homologs are R-loop readers acting to maintain genome stability (*55*), have been identified as the HRLP-associated proteins (table S1), implying that HRLP may coordinate molecular events pertaining to R-loop formation and its subsequent biological interpretation. Thus, our findings suggest a previously unidentified regulatory paradigm in which low splicing efficiency of *FLC* is associated with the formation of R-loop involving introns, thus impeding Pol II recruitment to repress *FLC* expression. Given the widespread cotranscriptionally splicing and R-loop structures in *Arabidopsis* (*44*, *56*, *57*), it would be intriguing to examine whether this regulatory paradigm represents a general mechanism in the whole transcriptome.

Notably, phase separation of HRLP is required for its function in suppressing splicing and transcription of *FLC* and the associated R-loop formation and impediment of RNA Pol II recruitment. This exemplifies that phase separation-mediated formation of nonmembrane cellular compartments could facilitate functional coupling of transcription and RNA processing (*58*). In agreement with the observations that the phase separation of RBPs is often driven by IDRs capable of weak multivalent interactions (*25*, *35*, *36*), our results demonstrate that HRLP undergoes phase separation to form nuclear condensates in vitro and in vivo through its IDR(4&5). Removal of IDR(4&5) compromises the formation of HRLP condensates, resulting in successive molecular and phenotypic changes as those displayed by *hrlp* loss-of-function mutants, including increased

splicing efficiency, reduced R-loop formation, enhanced RNA Pol II recruitment, and, consequently, late flowering. These causal links suggest that phase separation of HRLP is fundamental for its cellular function in suppressing *FLC* expression. HRLP condensates may serve as biological scaffolds that accommodate other regulatory components, including the splicing factor SR45 to enable efficient coupling of transcription and splicing of their downstream targets, such as the *FLC* pre-mRNA, and possibly other interacting partners to control various RNA processing steps in addition to splicing (fig. S8, L and M). While our study correlates the IDR-driven phase separation of HRLP with its function in mediating cotranscriptional splicing of *FLC*, further characterization of RNA binding proteome (*47*, *59*), including those associated with HRLP and *FLC*, will provide important insights into the mechanisms underlying the response of cellular RNA interactome to environmental and developmental signals.

## MATERIALS AND METHODS

### Plant materials and growth conditions

*Arabidopsis* plants were grown on Murashige and Skoog (MS) plates or soil under LDs (16-hour light/8-hour dark) or SDs (8-hour light/16-hour dark) at 23° ± 2°C, 16° ± 1°C, or 28° ± 2°C. The mutant seeds of *hrlp-1* (SALK_124411) and *sr45-1* (SALK_004132) in the Col background were obtained from the *Arabidopsis* Biological Resource Center (ABRC), and *hrlp-2* was generated by CRISPR-Cas9. *flc-3*, *ft-10*, *co-9*, *gi-1*, *fca-2*, *fpa-7*, *ld-1*, *fve-4*, *flk-2*, and *fld-3* mutants are in the Col background. Double mutants of *flc-3 hrlp-1*, *flc-3 hrlp-2*, and *sr45-1 hrlp-2* were generated by genetic crossing.

### Plasmid construction

To construct *g4HA-HRLP*, *gHRLP-GFP*, and *gHRLP-GUS*, the 5.0-kb *HRLP* genomic sequence was amplified and cloned into pENTR/D-TOPO (Invitrogen, catalog no. K240020) to generate *gHRLP*. The Spe I restriction site was introduced to *gHRLP* immediately after the start codon or before the stop codon by the QuikChange Site-Directed Mutagenesis Kit (Stratagene) to generate *g(SpeI)HRLP* or *gHRLP(SpeI)*, respectively. On the basis of these constructs, *g4HA-HRLP*, *gNLS-4HA-HRLP*, *gNES-4HA-HRLP*, *gHRLP-GFP*, and *gHRLP-GUS* were generated via cloning the corresponding sequences into the Spe I site. To construct *35S:GFP-HRLP* and *35S:GFP-HRLP* (truncated forms), the full-length coding sequence and various truncated sequences of *HRLP* were amplified and cloned into pGreen 0299 35S-GFP (*60*). To construct *GST-HRLP* or *GST-HRLP* (truncated forms), the full-length coding sequence and various truncated sequences of *HRLP* were amplified and cloned into pGEX-6p-2. To construct *35S:SR45-RFP*, the coding sequence of *SR45* was amplified and cloned into pGreen 0229-35S-RFP. The coding sequence of *SR45* was amplified and cloned into pENTR vector (*61*) harboring *9myc* to generate *35S:SR45-9myc*. To construct *gSR45-3myc*, the 4.3-kb *SR45* genomic sequence including 1.5-kb upstream region and 2.8-kb coding region plus introns was amplified and cloned into pENTR vector harboring 3myc. The primers used for plasmid construction are listed in table S2.

### Plant transformation

Transgenic plants were generated through the floral dipping method (*62*) using the *Agrobacterium* strain GV3101 harboring the desired constructs. *g4HA-HRLP*, *gNLS-4HA-HRLP*, *gNES-4HA-HRLP*, *gHRLP-GFP*, *pHRLP:GFP-HRLP*, *pHRLP:GFP-HRLP(ΔIDR4&5)*, *35S:GFP-HRLP*, and *35S:GFP-HRLP(ΔIDR4&5)* were transformed into *hrlp-2* mutants, while *gHRLP-GUS* was transformed into wild-type (Col) plants. *gSR45-3myc* was transformed into *sr45-1* mutants. These transgenic plants were all selected by Basta.

### Expression analysis

Total RNA was extracted from approximately 15 seedlings for each sample using the FavorPrep Plant Total RNA Mini Kit (Favorgen) and reverse-transcribed using the M-MLV Reverse Transcriptase System (Promega). qRT-PCR was performed with SYBR Green PCR Master Mix (Applied Biosystems, catalog no. A25742) on the 7900HT Fast Real-Time PCR system (Applied Biosystems). Gene expression was calculated as previously described (*61*). Primers used for gene expression analysis are listed in table S2. GUS staining was performed as previously described (*63*).

### In vitro RNA pull-down assay

The coding sequence of the triple RRM domain of HRLP was cloned into pGEX-6p-2 (Pharmacia). GST and GST-HRLP-RRM were expressed in *Escherichia coli* Rosetta (DE3) cells by induction with isopropyl-β-D-1-thiogalactopyranoside at 16°C overnight and purified with Glutathione Sepharose (GE Healthcare, catalog no. GE17-0756-05). The biotin-labeled *FLC* RNA probe was in vitro transcribed using T7 RNA polymerase (Roche, catalog no. 10881767001) and Biotin RNA Labelling Mix (Roche, catalog no. 11685597910) and pre-folded in RNA structure buffer [10 mM $MgCl_2$, 0.1 M KCl, and 10 mM tris-HCl (pH 7.0)]. The purified GST or GST-HRLP-RRM protein was incubated with the biotin-labeled *FLC* RNA probe for 1 hour, followed by incubation with Streptavidin Magnetic Beads (Roche, catalog no. 11641786001) overnight. The beads were extensively washed four times with 1× phosphate-buffered saline (PBS) buffer and boiled for 10 min, and the eluate was analyzed by Western blot using anti-GST antibody [Santa Cruz Biotechnology, sc-138 horseradish peroxidase (HRP), RRID:AB_627677].

### Systematic evolution of ligands by exponential enrichment

SELEX was performed as previously described with some modifications (*21*, *64*). The resulting matrix was in vitro transcribed into RNA population with T3 RNA polymerase (Promega, catalog no. P208C). After precipitation with ethanol, the RNA was dissolved in the binding buffer [20 mM Hepes (pH 7.9), 150 mM KCl, 1 mM dithiothreitol (DTT), tRNA (500 ng/ml), and 0.1% Triton X-100] and heated at 80°C for 5 min, followed by reducing the temperature to 22°C to allow the formation of the secondary structure. The resulting RNA and Recombinant RNasin Ribonuclease Inhibitor (Promega, catalog no. N2515) were incubated with GST or GST-HRLP bound to GST beads. The beads were then washed and treated with Proteinase K (Thermo Fisher Scientific, catalog no. 25530049) to release the bound RNA for further purification. The purified RNA was reverse-transcribed and amplified by PCR. The products from different amplification cycles were examined, and those from the minimum cycle showing a visible band were purified for subsequent selections. After seven rounds of selection, the final PCR products were ligated into pGEM-T vector (Promega, catalog no. A1360) and sequenced. Sequences were analyzed by MEME (http:/meme.nbcr.net/meme/). The primers used in SELEX are listed in table S2.

### Electrophoretic mobility shift assay

Biotin-labeled RNA (5′-Bio-YUCCUYCAYUCCUYCAYUCCUY-CAYUCCUYCA-3′) were incubated with GST or GST-HRLP protein in the binding buffer [10 mM Hepes (pH 7.3), 1 mM $MgCl_2$, 20 mM KCl, and 1 mM DTT] for 1 hour. For competition groups, the binding reaction occurred in the presence of different concentrations of unlabeled RNA probes. The mixture was separated on a 5% native polyacrylamide gel and transferred to the nylon membrane (GE Healthcare). After ultraviolet cross-linking, the membrane was detected with HRP-conjugated streptavidin (Thermo Fisher Scientific, catalog no. N100).

### Measurement of splicing efficiency

Total RNA extracted from seedlings were reverse-transcribed with a mixture of specified primers to obtain different forms of spliced and unspliced *FLC* isoforms. The ratios of spliced/unspliced of each isoform were calculated by dividing the value of spliced levels against that of the corresponding unspliced levels. The primers used are listed in table S2.

### Isolation of chromatin-bound RNA

Chromatin-bound RNA was isolated as previously described with some modifications (*65*). Around 300 individual seedlings were ground into powder and resuspended in Honda buffer [0.44 M sucrose, 10 mM $MgCl_2$, 20 mM Hepes, 1.25% (w/v) Ficoll, 2.5% (w/v) Dextran, 0.5% Triton X-100, 5 mM DTT, 1× proteinase inhibitor, ribonuclease (RNase) inhibitor (20 U/ml), and tRNA (50 ng/μl)]. The mixture was filtered with two layers of Miracloth followed by centrifugation. The pellet was resuspended in the resuspension buffer [25 mM tris-HCl (pH 7.5), 50% glycerol, 100 mM NaCl, 1 mM DTT, and 0.5 mM EDTA] and washed twice with the UREA wash buffer [0.5 mM EDTA, 25 mM tris-HCl (pH 7.5), 1% Tween 20, 1 mM DTT, 300 mM NaCl, and 1 M urea]. After eliminating DNA by deoxyribonuclease (DNase) I treatment, the chromatin-bound RNA was further purified for reverse transcription. The primers used for detecting nascent *FLC* expression are listed in table S2.

### RNA-seq and bioinformatics analysis

The aerial parts of 9-day-old wild-type and *hrlp-2* seedlings grown under LDs were harvested for total RNA extraction using the RNeasy Plus Mini kit (Qiagen) according to the manufacturer's instructions. The amount and quality of RNA were examined by gel electrophoresis and an Agilent Bioanalyzer 2100 system. rRNA was removed by a Ribo-Zero rRNA Removal kit (Eipcentre). The NEBNext Ultra II Directional RNA Library Prep Kit for Illumina (NEB) was used to construct the library, and sequencing was performed on the Illumina Novaseq 6000 platform. RNA-seq data were analyzed using Partek Flow (Partek). Briefly, paired-end raw reads were trimmed by removing reads with PHRED scores below 20 or with length shorter than 25 nt. Trimmed data were aligned to the reference genome TAIR10 using STAR 2.7.3a with default parameters. Filtered gene counts were normalized to the counts per million values. Differential gene expression analysis was performed using the Partek Gene Specific Analysis algorithm.

### RNA immunoprecipitation

RIP was carried out as previously described with some modifications (*66*). Around 300 individual seedlings were ground into powder and fixed with 1% formaldehyde for 10 min. The pellet was lysed in the lysis buffer [50 mM tris-HCl (pH 7.5), 150 mM NaCl, 4 mM $MgCl_2$, 0.25% Igepal CA-630, 1% SDS, 0.25% sodium deoxycholate, and 5 mM DTT] supplemented with RNase Inhibitor and Complete EDTA-free Protease Inhibitor Cocktail (Roche, catalog no. 5056489001). After preclearing with Protein A/G Plus Agarose (Santa Cruz Biotechnology, catalog no. sc-2003), the cell lysate was treated with Turbo DNase (Thermo Fisher Scientific, catalog no. AM2239) and RNase T1 (Thermo Fisher Scientific, catalog no. EN0541) for 15 min followed by incubation with anti-hemagglutinin (HA) agarose conjugate (Sigma-Aldrich, catalog no. A2095, RRID:AB_257974) for 3 hours at 4°C. RNA in the input and associated with beads was extracted using the RNeasy Plus Mini Kit (Qiagen) and reverse-transcribed using random hexamers (Invitrogen, catalog no. 51709). *TUB2* was included as an internal control. The primers used in RIP assay are listed in table S2.

### Chromatin immunoprecipitation

ChIP assay was performed as previously described (*67*). The chromatin extracted from around 300 individual seedlings was fixed and sonicated to produce DNA fragment at ~500 bp, followed by detection with anti-HA agarose conjugate (Sigma-Aldrich) or anti-RNA Pol II CTD antibody (Abcam, ab26721, RRID:AB_777726) bound to Protein A/G Plus Agarose Beads (Santa Cruz Biotechnology, catalog no. sc-2003). Fold enrichment of each fragment was determined by qRT-PCR, and a genomic fragment of *TUB2* was included as an internal control. The primers used in ChIP assay are listed in table S2.

### DNA-RNA immunoprecipitation

The nuclei from around 300 seedlings were isolated with the Honda buffer and treated with proteinase K in the lysis buffer [50 mM tris-HCl (pH 8.0), 10 mM EDTA, and 1% SDS] overnight. After purification, the DNA was treated with proteinase K for another 2 hours, followed by extraction and precipitation. The DNA pellet was dissolved in the lysis buffer and sonicated into fragments of ~500 bp. Purified DNA was immunoprecipitated with the S9.6 antibody (Kerafast, catalog no. ENH001, RRID:AB_2687463) bound to Protein A/G Plus Agarose Beads (Santa Cruz Biotechnology, catalog no. sc-2003) at 4°C overnight. The beads were subsequently washed thrice with wash buffer I [75 mM KCl, 50 mM tris (pH 8.0), 1% Triton X-100, and 0.1% sodium deoxycholate], once with wash buffer II [300 mM KCl, 50 mM tris (pH 8), 1% Triton X-100, and 0.1% sodium deoxycholate], and twice with wash buffer III [10 mM tris (pH 8) and 1 mM EDTA (pH 8)]. The DNA-RNA hybrid was eluted and purified with the PCR Purification Kit (Qiagen). For RNase H–treated samples, the sonicated DNA sample was treated with RNase H (NEB, catalog no. M0297S) at 37°C for 3 hours.

### R-loop foot-printing

R-loop foot-printing was performed as previously described (*42*). DNA was purified from around 300 9-day-old wild-type seedlings as described for the DRIP assay. After purification, 1.5 μg of DNA was treated with the bisulfite solution (EpiTect Bisulfite Kit, Qiagen) for at least 12 hours at 37°C. The modified DNA was amplified with primers Footp-C-F and Footp-R, and the resulting PCR products were ligated into the pGEM-T vector (Promega, catalog no. A1360). Around 15 individual clones were sequenced, and the sequencing data were aligned to the *FLC* genomic sequence. The primers are listed in table S2.

### CoIP coupled with LC-MS/MS analysis

Nuclear protein was isolated from seedlings using the nuclear isolation buffer [20 mM KCl, 25% glycerol, 20 mM tris (pH 7.0), 30 mM β-mercaptoethanol, 2.5 mM $MgCl_2$, 0.7% Triton X-100, 2 mM EDTA (pH 8.0), and 250 mM sucrose] with freshly added 1× protease inhibitor cocktail (Roche), and resuspended in IP buffer [50 mM Hepes (pH 7.5), 150 mM KCl, 10 μM $ZnSO_4$, 0.05% SDS, 5 mM $MgCl_2$, 1% Triton X-100, and 1× protease inhibitor cocktail], followed by incubation with anti-HA agarose conjugate (Sigma-Aldrich) for 4 hours at 4°C. After extensive washing, the immunoprecipitated proteins were eluted and analyzed by a TripleTOF5600 System (AB Sciex).

### Immunoblotting

Various proteins were resolved by SDS–polyacrylamide gel electrophoresis and detected using specific antibodies, including anti-HA (Santa Cruz Biotechnology, catalog no. sc-7392 HRP, RRID:AB_2894930), anti-myc (Santa Cruz Biotechnology, catalog no. sc-40, RRID:AB_627268), anti-GFP antibody (Santa Cruz Biotechnology, catalog no. sc-9996 HRP, RRID:AB_627695), and anti-H3 (Abcam, catalog no. ab1791, RRID:AB_302613) antibodies.

### In vitro phase separation assay

Various GST-tagged recombinant proteins, including GST-GFP, GST-GFP-HRLP, GST-GFP-HRLP(IDR4&5), GST-GFP-HRLP(ΔIDR4&5), and GST-RFP-SR45, were expressed in *E. coli* and purified with the Glutathione Sepharose beads (Amersham Bioscience). GST-free GFP fusion proteins were generated by PreScission Protease (GE Healthcare, catalog no. 27-0843-01) cleavage. Droplet assembly was performed with an addition of PEG-8000 (Sigma-Aldrich, catalog no. 25322-68-3) at a final concentration of 10% (w/v). The fluorescence was observed under an FV3000 Olympus confocal microscope.

### FRAP assay

FRAP was performed using a 40× oil immersion objective of the FV3000 Olympus confocal microscope. After nuclear bodies were bleached using the 488-nm laser, recovery was recorded every 5 or 10 s. Recovery curves were analyzed by the FV31S-SW software.

### Immunolocalization

Immunolocalization of 4HA-HRLP was performed as previously described (*68*, *69*). Protoplasts were isolated from 2-week-old *hrlp-2 g4HA-HRLP* and *hrlp-2* leaves, while roots were collected from 3-day-old *hrlp-2 g4HA-HRLP* and *hrlp-2* seedlings. Anti-HA (Santa Cruz Biotechnology, catalog no. sc-7392, RRID:AB_627809) and CF555 goat anti-mouse immunoglobulin G (IgG; Biotium, Cat# 20231, RRID:AB_10854844) antibodies were used as primary and secondary antibodies, respectively. The samples were examined with an FV3000 Olympus confocal microscope.

### Single-molecule RNA FISH

smFISH was performed as previously described (*70*) on root tips of 5-day-old *hrlp-2 gHRLP-GFP* seedlings using Quasar570-labeled probes against *FLC* intron I (*71*) (Biosearch Technologies). The samples were examined under an FV3000 Olympus confocal microscope.

## SUPPLEMENTARY MATERIALS

Supplementary material for this article is available at https://science.org/doi/10.1126/sciadv.abn5488

View/request a protocol for this paper from *Bio-protocol*.

## REFERENCES AND NOTES


1. G. Dreyfuss, V. N. Kim, N. Kataoka, Messenger-RNA-binding proteins and the messages they carry. *Nat. Rev. Mol. Cell Biol.* **3**, 195–205 (2002).
2. T. Geuens, D. Bouhy, V. Timmerman, The hnRNP family: Insights into their role in health and disease. *Hum. Genet.* **135**, 851–867 (2016).
3. C. G. Burd, G. Dreyfuss, Conserved structures and diversity of functions of RNA-binding proteins. *Science* **265**, 615–621 (1994).
4. B. M. Lunde, C. Moore, G. Varani, RNA-binding proteins: Modular design for efficient function. *Nat. Rev. Mol. Cell Biol.* **8**, 479–490 (2007).
5. A. Clery, M. Blatter, F. H. Allain, RNA recognition motifs: Boring? Not quite. *Curr. Opin. Struct. Biol.* **18**, 290–298 (2008).
6. R. Valverde, L. Edwards, L. Regan, Structure and function of KH domains. *FEBS J.* **275**, 2712–2726 (2008).
7. J. Font, J. P. Mackay, Beyond DNA: Zinc finger domains as RNA-binding modules. *Methods Mol. Biol.* **649**, 479–491 (2010).
8. C. Maris, C. Dominguez, F. H. Allain, The RNA recognition motif, a plastic RNA-binding platform to regulate post-transcriptional gene expression. *FEBS J.* **272**, 2118–2131 (2005).
9. Z. J. Lorkovic, A. Barta, Genome analysis: RNA recognition motif (RRM) and K homology (KH) domain RNA-binding proteins from the flowering plant *Arabidopsis thaliana*. *Nucleic Acids Res.* **30**, 623–635 (2002).
10. W. Prall, B. Sharma, B. D. Gregory, Transcription is just the beginning of gene expression regulation: The functional significance of RNA-Binding proteins to post-transcriptional processes in plants. *Plant Cell Physiol.* **60**, 1939–1952 (2019).
11. T. Glisovic, J. L. Bachorik, J. Yong, G. Dreyfuss, RNA-binding proteins and post-transcriptional gene regulation. *FEBS Lett.* **582**, 1977–1986 (2008).
12. E. Martinez-Salas, G. Lozano, J. Fernandez-Chamorro, R. Francisco-Velilla, A. Galan, R. Diaz, RNA-binding proteins impacting on internal initiation of translation. *Int. J. Mol. Sci.* **14**, 21705–21726 (2013).
13. S. Bao, C. Hua, L. Shen, H. Yu, New insights into gibberellin signaling in regulating flowering in Arabidopsis. *J. Integr. Plant Biol.* **62**, 118–131 (2020).
14. H. Cho, H. S. Cho, I. Hwang, Emerging roles of RNA-binding proteins in plant development. *Curr. Opin. Plant Biol.* **51**, 51–57 (2019).
15. G. G. Simpson, C. Dean, *Arabidopsis*, the Rosetta stone of flowering time? *Science* **296**, 285–289 (2002).
16. C. Liu, Z. Thong, H. Yu, Coming into bloom: The specification of floral meristems. *Development* **136**, 3379–3391 (2009).
17. C. Whittaker, C. Dean, The FLC locus: A platform for discoveries in epigenetics and adaptation. *Annu. Rev. Cell Dev. Biol.* **33**, 555–575 (2017).
18. C. Hornyik, L. C. Terzi, G. G. Simpson, The spen family protein FPA controls alternative cleavage and polyadenylation of RNA. *Dev. Cell* **18**, 203–213 (2010).
19. F. Liu, S. Marquardt, C. Lister, S. Swiezewski, C. Dean, Targeted 3′ processing of antisense transcripts triggers *Arabidopsis FLC* chromatin silencing. *Science* **327**, 94–97 (2010).
20. Q. Yan, X. Xia, Z. Sun, Y. Fang, Depletion of *Arabidopsis* SC35 and SC35-like serine/arginine-rich proteins affects the transcription and splicing of a subset of genes. *PLOS Genet.* **13**, e1006663 (2017).
21. Z. Wu, D. Zhu, X. Lin, J. Miao, L. Gu, X. Deng, Q. Yang, K. Sun, D. Zhu, X. Cao, T. Tsuge, C. Dean, T. Aoyama, H. Gu, L. J. Qu, RNA binding proteins RZ-1B and RZ-1C play critical roles in regulating pre-mRNA splicing and gene expression during development in Arabidopsis. *Plant Cell* **28**, 55–73 (2016).
22. S. Rosa, S. Duncan, C. Dean, Mutually exclusive sense-antisense transcription at *FLC* facilitates environmentally induced gene repression. *Nat. Commun.* **7**, 13031 (2016).
23. H. J. Wiedner, J. Giudice, It's not just a phase: Function and characteristics of RNA-binding proteins in phase separation. *Nat. Struct. Mol. Biol.* **28**, 465–473 (2021).
24. S. E. Liao, O. Regev, Splicing at the phase-separated nuclear speckle interface: A model. *Nucleic Acids Res.* **49**, 636–645 (2021).
25. Y. Lin, D. S. Protter, M. K. Rosen, R. Parker, Formation and maturation of phase-separated liquid droplets by RNA-binding proteins. *Mol. Cell* **60**, 208–219 (2015).
26. S. Alberti, A. Gladfelter, T. Mittag, Considerations and challenges in studying liquid-liquid phase separation and biomolecular condensates. *Cell* **176**, 419–434 (2019).
27. S. K. Powers, A. S. Holehouse, D. A. Korasick, K. H. Schreiber, N. M. Clark, H. Jing, R. Emenecker, S. Han, E. Tycksen, I. Hwang, R. Sozzani, J. M. Jez, R. V. Pappu, L. C. Strader, Nucleo-cytoplasmic partitioning of ARF proteins controls auxin responses in *Arabidopsis thaliana*. *Mol. Cell* **76**, 177–190.e5 (2019).
28. X. Fang, L. Wang, R. Ishikawa, Y. Li, M. Fiedler, F. Liu, G. Calder, B. Rowan, D. Weigel, P. Li, C. Dean, *Arabidopsis* FLL2 promotes liquid-liquid phase separation of polyadenylation complexes. *Nature* **569**, 265–269 (2019).
29. M. Ouyang, X. Li, J. Zhang, P. Feng, H. Pu, L. Kong, Z. Bai, L. Rong, X. Xu, W. Chi, Q. Wang, F. Chen, C. Lu, J. Shen, L. Zhang, Liquid-liquid phase transition drives intra-chloroplast cargo sorting. *Cell* **180**, 1144–1159.e20 (2020).

30. J. H. Jung, A. D. Barbosa, S. Hutin, J. R. Kumita, M. Gao, D. Derwort, C. S. Silva, X. Lai, E. Pierre, F. Geng, S. B. Kim, S. Baek, C. Zubieta, K. E. Jaeger, P. A. Wigge, A prion-like domain in ELF3 functions as a thermosensor in *Arabidopsis*. *Nature* **585**, 256–260 (2020).
31. R. Zavaliev, R. Mohan, T. Chen, X. Dong, Formation of NPR1 condensates promotes cell survival during the plant immune response. *Cell* **182**, 1093–1108.e18 (2020).
32. D. Xie, M. Chen, J. Niu, L. Wang, Y. Li, X. Fang, P. Li, Y. Qi, Phase separation of SERRATE drives dicing body assembly and promotes miRNA processing in *Arabidopsis*. *Nat. Cell Biol.* **23**, 32–39 (2021).
33. C. A. Helliwell, C. C. Wood, M. Robertson, W. James Peacock, E. S. Dennis, The *Arabidopsis* FLC protein interacts directly in vivo with *SOC1* and *FT* chromatin and is part of a high-molecular-weight protein complex. *Plant J.* **46**, 183–192 (2006).
34. P. Li, Z. Tao, C. Dean, Phenotypic evolution through variation in splicing of the noncoding RNA COOLAIR. *Genes Dev.* **29**, 696–701 (2015).
35. P. A. Chong, J. D. Forman-Kay, Liquid-liquid phase separation in cellular signaling systems. *Curr. Opin. Struct. Biol.* **41**, 180–186 (2016).
36. C. P. Brangwynne, P. Tompa, R. V. Pappu, Polymer physics of intracellular phase transitions. *Nat. Phys.* **11**, 899–904 (2015).
37. A. Castello, B. Fischer, K. Eichelbaum, R. Horos, B. M. Beckmann, C. Strein, N. E. Davey, D. T. Humphreys, T. Preiss, L. M. Steinmetz, J. Krijgsveld, M. W. Hentze, Insights into RNA biology from an atlas of mammalian mRNA-binding proteins. *Cell* **149**, 1393–1406 (2012).
38. A. K. Lancaster, A. Nutter-Upham, S. Lindquist, O. D. King, PLAAC: A web and command-line application to identify proteins with prion-like amino acid composition. *Bioinformatics* **30**, 2501–2502 (2014).
39. G. S. Ali, S. G. Palusa, M. Golovkin, J. Prasad, J. L. Manley, A. S. Reddy, Regulation of plant developmental processes by a novel splicing factor. *PLOS ONE* **2**, e471 (2007).
40. A. Aguilera, T. Garcia-Muse, R loops: From transcription byproducts to threats to genome stability. *Mol. Cell* **46**, 115–124 (2012).
41. K. Skourti-Stathaki, N. J. Proudfoot, A double-edged sword: R loops as threats to genome integrity and powerful regulators of gene expression. *Genes Dev.* **28**, 1384–1396 (2014).
42. Q. Sun, T. Csorba, K. Skourti-Stathaki, N. J. Proudfoot, C. Dean, R-loop stabilization represses antisense transcription at the *Arabidopsis FLC* locus. *Science* **340**, 619–621 (2013).
43. C. Xu, Z. Wu, H. C. Duan, X. Fang, G. Jia, C. Dean, R-loop resolution promotes co-transcriptional chromatin silencing. *Nat. Commun.* **12**, 1790 (2021).
44. W. Xu, H. Xu, K. Li, Y. Fan, Y. Liu, X. Yang, Q. Sun, The R-loop is a common chromatin feature of the *Arabidopsis* genome. *Nat. Plants* **3**, 704–714 (2017).
45. N. Geraldo, I. Baurle, S. Kidou, X. Hu, C. Dean, FRIGIDA delays flowering in *Arabidopsis* via a cotranscriptional mechanism involving direct interaction with the nuclear cap-binding complex. *Plant Physiol.* **150**, 1611–1618 (2009).
46. G. Dreyfuss, M. J. Matunis, S. Pinol-Roma, C. G. Burd, hnRNP proteins and the biogenesis of mRNA. *Annu. Rev. Biochem.* **62**, 289–321 (1993).
47. T. Koster, C. Marondedze, K. Meyer, D. Staiger, RNA-binding proteins revisited—The emerging *Arabidopsis* mRNA interactome. *Trends Plant Sci.* **22**, 512–526 (2017).
48. A. R. Kornblihtt, M. de la Mata, J. P. Fededa, M. J. Munoz, G. Nogues, Multiple links between transcription and splicing. *RNA* **10**, 1489–1498 (2004).
49. D. L. Bentley, Coupling mRNA processing with transcription in time and space. *Nat. Rev. Genet.* **15**, 163–175 (2014).
50. Y. Zhang, Y. Ding, The simultaneous coupling of transcription and splicing in plants. *Mol. Plant* **13**, 184–186 (2020).
51. X. Ji, Y. Zhou, S. Pandit, J. Huang, H. Li, C. Y. Lin, R. Xiao, C. B. Burge, X. D. Fu, SR proteins collaborate with 7SK and promoter-associated nascent RNA to release paused polymerase. *Cell* **153**, 855–868 (2013).
52. R. Das, J. Yu, Z. Zhang, M. P. Gygi, A. R. Krainer, S. P. Gygi, R. Reed, SR proteins function in coupling RNAP II transcription to pre-mRNA splicing. *Mol. Cell* **26**, 867–881 (2007).
53. M. de la Mata, A. R. Kornblihtt, RNA polymerase II C-terminal domain mediates regulation of alternative splicing by SRp20. *Nat. Struct. Mol. Biol.* **13**, 973–980 (2006).
54. M. Monsalve, Z. Wu, G. Adelmant, P. Puigserver, M. Fan, B. M. Spiegelman, Direct coupling of transcription and mRNA processing through the thermogenic coactivator PGC-1. *Mol. Cell* **6**, 307–316 (2000).
55. W. Yuan, J. Zhou, J. Tong, W. Zhuo, L. Wang, Y. Li, Q. Sun, W. Qian, ALBA protein complex reads genic R-loops to maintain genome stability in *Arabidopsis*. *Sci. Adv.* **5**, eaav9040 (2019).
56. D. Zhu, F. Mao, Y. Tian, X. Lin, L. Gu, H. Gu, L. J. Qu, Y. Wu, Z. Wu, The features and regulation of co-transcriptional splicing in *Arabidopsis*. *Mol. Plant* **13**, 278–294 (2020).
57. S. Li, Y. Wang, Y. Zhao, X. Zhao, X. Chen, Z. Gong, Global co-transcriptional splicing in *Arabidopsis* and the correlation with splicing regulation in mature RNAs. *Mol. Plant* **13**, 266–277 (2020).
58. J. Yang, Y. Cao, L. Ma, Co-transcriptional RNA processing in plants: Exploring from the perspective of polyadenylation. *Int. J. Mol. Sci.* **22**, 3300 (2021).
59. M. Bach-Pages, F. Homma, J. Kourelis, F. Kaschani, S. Mohammed, M. Kaiser, R. A. L. van der Hoorn, A. Castello, G. M. Preston, Discovering the RNA-binding proteome of plant leaves with an improved RNA interactome capture method. *Biomolecules* **10**, 661 (2020).
60. L. Shen, Z. Liang, X. Gu, Y. Chen, Z. W. Teo, X. Hou, W. M. Cai, P. C. Dedon, L. Liu, H. Yu, $N^6$-methyladenosine RNA modification regulates shoot stem cell fate in *Arabidopsis*. *Dev. Cell* **38**, 186–200 (2016).
61. Y. Chen, S. Song, Y. Gan, L. Jiang, H. Yu, L. Shen, SHAGGY-like kinase 12 regulates flowering through mediating CONSTANS stability in *Arabidopsis*. *Sci. Adv.* **6**, eaaw0413 (2020).
62. S. J. Clough, A. F. Bent, Floral dip: A simplified method for *Agrobacterium*-mediated transformation of *Arabidopsis thaliana*. *Plant J.* **16**, 735–743 (1998).
63. L. Shen, Z. Thong, X. Gong, Q. Shen, Y. Gan, H. Yu, The putative PRC1 RING-finger protein AtRING1A regulates flowering through repressing *MADS AFFECTING FLOWERING* genes in *Arabidopsis*. *Development* **141**, 1303–1312 (2014).
64. Y. Cavaloc, C. F. Bourgeois, L. Kister, J. Stévenin, The splicing factors 9G8 and SRp20 transactivate splicing through different and specific enhancers. *RNA* **5**, 468–483 (1999).
65. Z. Wu, R. Ietswaart, F. Liu, H. Yang, M. Howard, C. Dean, Quantitative regulation of *FLC* via coordinated transcriptional initiation and elongation. *Proc. Natl. Acad. Sci. U.S.A.* **113**, 218–223 (2016).
66. K. Meyer, T. Koster, C. Nolte, C. Weinholdt, M. Lewinski, I. Grosse, D. Staiger, Adaptation of iCLIP to plants determines the binding landscape of the clock-regulated RNA-binding protein AtGRP7. *Genome Biol.* **18**, 204 (2017).
67. L. Shen, Y. G. Kang, L. Liu, H. Yu, The J-domain protein J3 mediates the integration of flowering signals in Arabidopsis. *Plant Cell* **23**, 499–514 (2011).
68. M. H. Lee, Y. Lee, I. Hwang, In vivo localization in Arabidopsis protoplasts and root tissue. *Methods Mol. Biol.* **1043**, 113–120 (2013).
69. L. Shen, Y. Zhang, N. Sawettalake, A molecular switch for *FLOWERING LOCUS C* activation determines flowering time in Arabidopsis. *Plant Cell* **34**, 818–833 (2022).
70. S. Duncan, T. S. G. Olsson, M. Hartley, C. Dean, S. Rosa, Single molecule RNA FISH in Arabidopsis root cells. *Bio. Protoc.* **7**, e2240 (2017).
71. R. Ietswaart, S. Rosa, Z. Wu, C. Dean, M. Howard, Cell-size-dependent transcription of FLC and its antisense long non-coding RNA COOLAIR explain cell-to-cell expression variation. *Cell Syst.* **4**, 622–635.e9 (2017).


**Acknowledgments:** We thank G. B. Chen for analyzing the RNA-seq data, and the Protein and Proteomics Centre (PPC) in the Department of Biological Sciences, National University of Singapore for the LC-MS/MS service. **Funding:** This work was supported by the National Research Foundation Competitive Research Programme (NRF-CRP22-2019-0001), Singapore Food Story R&D Programme (SFS_RND_SUFP_001_04), and the intramural research support from Temasek Life Sciences Laboratory and National University of Singapore. **Author contributions:** Y.Z., L.S., and H.Y. conceived this study and designed the experiments. Y.Z., S.F., C.H., Z.W.N.T., J.X.K., and L.S. performed the experiments. Y.Z., L.S., and H.Y. analyzed data and wrote the paper. All authors read and approved the manuscript. **Competing interests:** The authors declare that they have no competing interests. **Data and materials availability:** All data needed to evaluate the conclusions in the paper are present in the paper and/or the Supplementary Materials. Sequencing reads are available in the National Center for Biotechnology Information (NCBI) Gene Expression Omnibus (GEO) database (accession no. GSE200390). Request for plant materials should be submitted to H.Y. (dbsyuhao@nus.edu.sg).

Submitted 3 December 2021
Accepted 6 May 2022
Published 22 June 2022
10.1126/sciadv.abn5488